Journal of Fluids and Structures 49 (2014) 91–111

Contents lists available at ScienceDirect

Journal of Fluids and Structures

journal homepage: www.elsevier.com/locate/jfs

Improving vortex models via optimal control theory

Maziar S. Hemati *, Jeff D. Eldredge, Jason L. Speyer

Department of Mechanical and Aerospace Engineering, University of California, Los Angeles, CA 90095, USA

ARTICLE INFO

Article history:
Received 27 June 2013
Accepted 13 April 2014
Available online 16 May 2014

Keywords:
Model optimization
Optimal control
Point vortex
Unsteady aerodynamics

ABSTRACT

Low-order inviscid point vortex models have demonstrated success in capturing the qualitative behavior of aerodynamic forces resulting from unsteady lifting surface maneuvers. However, the quantitative agreement is often lacking for separated flows as a result of the ambiguity in the edge conditions in this fundamentally unsteady process. In this work, we develop a model reduction framework in which such models can be systematically improved with empirical results. We consider the low-order impulse matching vortex model in which, in its original form, Kutta conditions are applied at both edges to determine the strengths of single point vortices shed from each edge. Here, we relax the Kutta condition imposed at the plate's edges and instead seek the time rate of change of the vortex strengths that minimize the discrepancy between the model-predicted and high-fidelity simulation force histories, while the vortex positions adhere to the dynamics of the low-order model. A constrained minimization problem is constructed within an optimal control framework and solved by means of variational principles. The optimization approach is demonstrated on several unsteady wing maneuvers, including pitch-up and impulsive translation at a fixed angle of attack. Additionally, a stitching technique is introduced for extending the time interval over which the model is optimized.

1. Introduction

An improved understanding of the unsteady effects associated with high angle of attack maneuvers has great potential for advancing the capabilities of modern flight systems. For example, by exploiting the leading edge vortex (LEV), an aircraft may be able to realize increased lift or maneuverability by means of delayed stall. Despite recent advances in the field of unsteady aerodynamics, however, low-order models for predicting the aerodynamic forces and moments are still inadequate for designing reliable flight control systems for successfully conducting agile maneuvers. A primary contributor to this shortcoming is a lack of low-dimensional aerodynamic models capable of reliably predicting forces and moments over a wide-range of kinematics.

Low-order modeling of unsteady aerodynamics initially started with the work of Wagner (1925) and Theodorsen (1935). These early studies established a precedent for analyzing such problems by decomposing the forces and moments on the wing into contributions from circulatory (i.e., vortex induced) and non-circulatory (i.e., inertial reaction, or added mass) effects. Many researchers have taken similar phenomenological approaches to modeling. For example, an assortment of

* Corresponding author. Present address: Department of Mechanical and Aerospace Engineering, Princeton University, Princeton, NJ 08544, USA. Tel.: +1 408 761 5001.
E-mail address: mhemati@princeton.edu (M.S. Hemati).

http://dx.doi.org/10.1016/j.jfluidstructs.2014.04.004
0889-9746/

Nomenclature

a	semi-chord of plate
c	chord of plate
C_d	drag coefficient
C_l	lift coefficient
F_x, F_y	components of force
$\mathcal{H}$	optimization Hamiltonian
J	objective function
K	dimensionless pitch rate, $\dot{\alpha}_0 c/(2U)$
$\mathbf{p}$	optimization costate vector
Re	Reynolds number
$\mathbf{u}$	optimization input vector
U	speed of translation
$\mathbf{x}$	optimization state vector
$\mathbf{x}_o$	optimization initial state vector
z	complex coordinate, $x+iy$, in physical plane
$\tilde{z}$	plate-fixed coordinates
z_c	plate centroid
z_ν	position of vortex ν in physical plane
$z_{\nu 0}$	position of the releasing edge of vortex ν
α	angle of attack
$\dot{\alpha}_0$	nominal dimensional pitch rate
Γ_ν	strength of vortex ν
ϵ	gradient descent threshold stopping criterion
ζ	complex coordinate, $\xi+i\eta$, in circle plane
ζ_ν	position of vortex ν in circle plane
θ	angular coordinate in circle plane
κ_i	gradient descent step size for parameter i
ν	fluid kinematic viscosity
ρ	fluid density

vortex models have been developed to account for the shed vorticity through a multitude of simple vortex representations, such as vortex sheets (Wagner, 1925; Theodorsen, 1935; Garrick, 1937; von Kármán and Sears, 1938; Krasny, 1991; Nitsche and Krasny, 1994; Jones, 2003; Pullin and Wang, 2004; Shukla and Eldredge, 2007; Alben and Shelley, 2008), continuous sequences of point vortices (Katz and Weihs, 1978; Jones and Platzer, 2000; Ansari et al., 2006; Ramesh et al., 2013; Xia and Mohseni, 2013), or finite sets of point vortices with evolving strengths (Brown and Michael, 1954; Graham, 1980; Cortelezzi and Leonard, 1993; Michelin and Llewelyn Smith, 2009; Wang and Eldredge, 2013).

Many of these classical potential flow models perform well for low angles of attack, but fail to provide reliable force predictions when the angle of attack is increased to the point that the LEV plays a significant role. The impulse matching model, a low-order variable-strength vortex model, has recently been developed to address this issue (Wang and Eldredge, 2013). The model, which makes use of a Kutta condition at the wing's leading and trailing edges in order to determine the strengths of evolving point vortices, provides reasonable force predictions in many cases; however, the model still remains inadequate for aerodynamic control and estimation. This is not entirely surprising, since the Kutta conditions are primarily used due to the lack of a better model. In reality viscous and curvature effects play a significant role, especially at the leading edge, thus making the Kutta condition an ill-suited model for maneuvers with LEV development.

It may be possible to circumvent these modeling deficiencies by synthesizing empirical data to construct a more reliable alternative. For example, several researchers have successfully improved upon template models by tailoring them based on relevant empirical data. In one such model, experimental force data is used to determine the strengths and positions of a set of stationary point vortices (Pitt Ford and Babinsky, 2013). Similarly, Wong et al. (2013) implement a vortex-feeding model to estimate the time-varying circulation of a wing from time-resolved measurements of the leading edge shear layer velocity profile. Another example, from Brunton and Rowley (2011, 2013), makes use of an empirically determined Theodorsen function to improve upon Theodorsen's classical lift model. Ramesh et al. (2012) augment a point vortex model with an empirically determined leading edge suction parameter to govern vortex shedding from the leading edge of an airfoil. Additionally, the method of indicial responses, considered in Leishman and Beddoes (1989) and more recently in Taha et al. (2013), enables the construction of empirically guided models capable of reasonable force and moment predictions.

In the present work, we develop a general framework for exploiting empirical data to improve upon existing vortex models. Specifically, we relax the Kutta conditions imposed at the leading and trailing edges of the impulse matching vortex model (Wang and Eldredge, 2013) and instead determine the vortex strengths by minimizing the difference between some model predicted and high-fidelity simulation metric (here, force). The minimization is constrained to ensure that vortices move according to specified dynamical equations. Although the resulting model is not autonomous, it provides insight into the deficiencies of the original model and may guide future model development.

We summarize the impulse matching model in Section 2, which will serve as the baseline vortex model for the minimization procedure. The minimization problem is formulated in Section 3, which also details the method of solution and the viscous vortex particle method used in acquiring “truth” data for the optimization procedure. In Section 4 we apply the optimization procedure to two canonical wing maneuvers: (1) pitch-up and (2) impulsive translation at a fixed angle of attack. Finally, in Section 5, we discuss some of the remaining challenges in vortex model optimization.

2. Vortex model overview

In the present section, we briefly introduce the impulse matching model for predicting the aerodynamic forces of a pitching and/or translating airfoil. A more detailed development can be found in Wang and Eldredge (2013).

The model formulation makes use of complex potentials, such that the infinitely thin plate can be mapped from the circle plane (i.e., $\zeta = \xi + i\eta$) to the physical plane (i.e., $z = x + iy$) via the Joukowski mapping, as depicted in Fig. 1. The complex mapping for a plate of semi-chord a can be expressed as

$$z(\zeta) = z_c + \tilde{z}(\zeta)e^{i\alpha}, \tag{1}$$

where

$$\tilde{z}(\zeta) = \frac{a}{2}\left(\zeta + \frac{1}{\zeta}\right). \tag{2}$$

The plate is mapped from a circle of unit radius in the ζ-plane, that is, $\zeta = e^{i\theta}$ describes its surface for $\theta = [0, 2\pi)$. The leading edge is denoted by z_{10}, which is located at $\zeta = 1$ (i.e., $\tilde{z}_{10} = a$). Similarly, the trailing edge is denoted by z_{20} which corresponds to $\zeta = -1$ (i.e., $\tilde{z}_{20} = -a$).

Cumulative vorticity production is modeled by means of a point vortex of variable strength associated with each of the salient edges. The vortex equations of motion in the presence of a body follow the impulse matching model, based on the principle that any time variation of the strength of a point vortex should have no direct effect on the force (Wang and Eldredge, 2013). The resulting equations of motion for the vortex system have the general form

$$\frac{d\mathbf{x}}{dt} = \mathbf{f}(\mathbf{x}, \mathbf{u}, t), \tag{3}$$

where $\mathbf{x}$ consists of the vortex coordinates and strengths, while $\mathbf{u}$ represents a vector of the time rate of change of the vortex strengths.

For a flat plate with a leading and trailing edge, two developing vortices are considered in addition to any vortices already existing in the flow. The strengths of these developing point vortices are determined by applying a Kutta condition at each edge. This can be expressed as a set of constraints

$$h(\mathbf{x}, \mathbf{u}, t) = 0, \tag{4}$$

which ensures that the flow remains finite at $\zeta_{10} = 1$ and $\zeta_{20} = -1$.

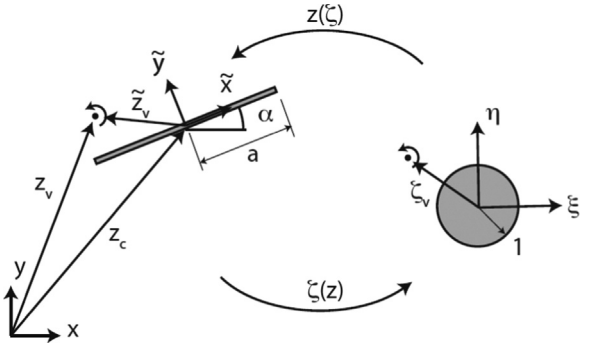

Fig. 1. Schematic of plate mapping to circle of unit radius in the ζ-plane.

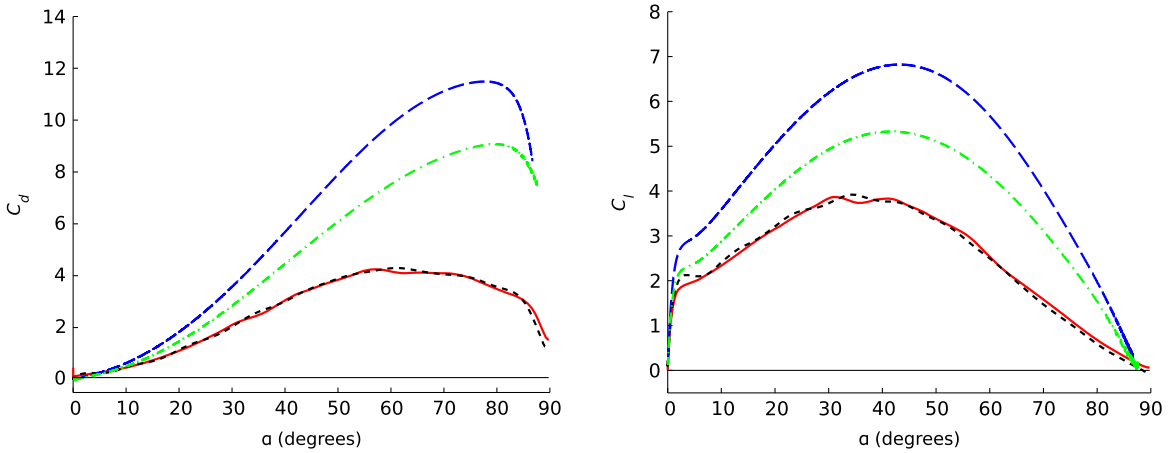

Fig. 2. Comparison of the force histories for a pitch-up maneuver with reduced frequency $K = 0.2$, as defined in Section 4.1. Results correspond to the Brown–Michael vortex model (– –), the impulse matching model (– · –), the viscous vortex particle method (——), and the experiments of Granlund et al. (2010) (- - -). Figure courtesy from Wang and Eldredge (2013).

The capabilities of the impulse matching model are showcased in Wang and Eldredge (2013). Significant improvements are made over the Brown–Michael vortex model, used in Eldredge and Wang (2010), for the same canonical maneuvers. Fig. 2, adapted from Wang and Eldredge (2013), provides a comparison of both low-order models with respect to high fidelity numerical results (Re = 1000) as well as experimental results (Re = 20 000). It is clear that there is still significant room for making model improvements. In the next section, we develop an approach grounded in optimal control theory to guide these efforts.

3. A variational approach to vortex model improvement

The impulse matching model leads to reasonable aerodynamic force predictions under many circumstances, but these predictions are still inadequate for the purposes of aerodynamic control. In the present section, we seek to improve this model by formulating a constrained minimization problem with free initial states. We outline the steepest descent algorithm used in solving the optimization problem, and we discuss the high-fidelity computations used in determining the true force histories against which the optimization is conducted.

3.1. Constrained optimization formulation

Here, we seek to improve the impulse matching model by relaxing the Kutta condition at both edges. With no conditions imposed on the vortex strengths, we can determine the time rate of change of these strengths such that the model force predictions more accurately represent the true aerodynamic forces observed. To do so, we consider the nonlinear continuous-time optimal control problem with fixed initial and terminal times. We seek the optimal control history $\mathbf{u}^*(t)$ and the optimal initial state $\mathbf{x}_o^*$ that minimize the mean squared error between the true and the model-predicted force histories, while adhering to the governing equations of the vortex model. That is, we seek the minimum cost

$$J^* = \min_{\mathbf{u},\mathbf{x}_o} \int_{t_o}^{t_f} g(\mathbf{x},\mathbf{u},t)\,\mathrm{d}t, \tag{5}$$

where

$$g(\mathbf{x},\mathbf{u},t) := [F_x^{\text{true}}(t) - F_x^{\text{model}}(\mathbf{x},\mathbf{u},t)]^2 + [F_y^{\text{true}}(t) - F_y^{\text{model}}(\mathbf{x},\mathbf{u},t)]^2, \tag{6}$$

subject to the vortex evolution equations imposed by the impulse matching model

$$\frac{\mathrm{d}\mathbf{x}}{\mathrm{d}t} = \mathbf{f}(\mathbf{x},\mathbf{u},t) \tag{7}$$

and the initial state

$$\mathbf{x}(t_o) = \mathbf{x}_o. \tag{8}$$

The state and input vectors are defined, respectively, as

$$\mathbf{x}(t) := [\xi_1\ \eta_1\ \xi_2\ \eta_2\ \Gamma_1\ \Gamma_2]^{\mathsf{T}} \in \mathbb{R}^6 \tag{9}$$

and

$$\mathbf{u}(t) := [\dot{\Gamma}_1\ \dot{\Gamma}_2]^{\mathsf{T}} \in \mathbb{R}^2, \tag{10}$$

where $\zeta_\nu = \xi_\nu + i\eta_\nu$ corresponds to the position coordinates of vortex ν in the circle plane, and $\dot{\Gamma}_\nu$ denotes the rate of change in the strength of vortex ν. Here, the right hand side of the state update equation (7) follows the impulse matching model for the vortex positions, while the strength propagation of each vortex ν is determined from the control input $\dot{\Gamma}_\nu$. It is emphasized that other vortex models may be used in lieu of the impulse matching model used here, and one could also conceive other choices for the cost function.

To solve the above minimization, we construct the Hamiltonian for this system (Bryson and Ho, 1975; Kirk, 2004; Speyer and Jacobson, 2010)

$$\mathcal{H} = g(\mathbf{x},\mathbf{u},t) + \mathbf{p}(t)^{\mathsf{T}}\mathbf{f}(\mathbf{x},\mathbf{u},t), \tag{11}$$

where $\mathbf{p}(t) \in \mathbb{R}^6$ represents the costate of the system, corresponding to the marginal cost of violating the system constraints. We then seek the optimal input history $\mathbf{u}^*(t)$ and the optimal initial state vector $\mathbf{x}_o^*$ such that the first order necessary conditions for optimality are satisfied. That is, we solve

$$\dot{\mathbf{x}} = \frac{\partial \mathcal{H}}{\partial \mathbf{p}}(\mathbf{x},\mathbf{u},t) = \mathbf{f}(\mathbf{x},\mathbf{u},t), \tag{12}$$

$$\dot{\mathbf{p}} = -\frac{\partial \mathcal{H}}{\partial \mathbf{x}}(\mathbf{x},\mathbf{u},t) = -\frac{\partial g}{\partial \mathbf{x}}(\mathbf{x},\mathbf{u},t) - \left[\frac{\partial \mathbf{f}}{\partial \mathbf{x}}(\mathbf{x},\mathbf{u},t)\right]^{\mathsf{T}} \mathbf{p}(t), \tag{13}$$

with the optimality conditions

$$0 = \frac{\partial \mathcal{H}}{\partial \mathbf{u}}(\mathbf{x}, \mathbf{u}, t) = \frac{\partial g}{\partial \mathbf{u}}(\mathbf{x}, \mathbf{u}, t) + \left[\frac{\partial \mathbf{f}}{\partial \mathbf{u}}(\mathbf{x}, \mathbf{u}, t)\right]^{\mathsf{T}} \mathbf{p}(t), \tag{14}$$

$$0 = \frac{\partial J}{\partial \mathbf{x}_o}. \tag{15}$$

Minimizations with respect to both $\mathbf{u}$ and $\mathbf{x}_o$ are conducted by means of the steepest descent algorithm, outlined in Section 3.2.

3.2. Method of solution

The steepest descent algorithm, tailored to our problem of interest, consists of five steps as follows (Bryson and Ho, 1975; Kirk, 2004; Speyer and Jacobson, 2010):

1. Uniformly discretize the time interval $[t_o, t_f]$ into N equal subintervals and assume that the control takes the form of a zero-order hold for an initial guess $\mathbf{u}^{(i=0)}(t) = \mathbf{u}^{(i=0)}(t_k)$, $t \in [t_k, t_{k+1}]$, $k = 0, 1, \ldots, N-1$.
2. Apply the assumed control sequence $\mathbf{u}^{(i)}(t)$ to integrate the state equations forward in time from t_o to t_f with the current iteration of the initial conditions $\mathbf{x}(0) = \mathbf{x}_o^{(i)}$ and store the state trajectory $\mathbf{x}^{(i)}(t)$.
3. Apply both $\mathbf{u}^{(i)}(t)$ and $\mathbf{x}^{(i)}(t)$ to integrate the costate equations backward in time from t_f to t_o, where the terminal value of the costate is $\mathbf{p}^{(i)}(t_f) = 0$.
4. Evaluate and store both $\partial J^{(i)}/\partial \mathbf{x}_o$ and $\partial \mathcal{H}^{(i)}(t)/\partial \mathbf{u}$, $t \in [t_o, t_f]$.
5. Evaluate the stopping criterion and stop the iterative procedure when

$$\left\| \frac{\partial \mathcal{H}^{(i)}}{\partial \mathbf{u}} \right\| = \left\{ \int_{t_o}^{t_f} [\partial \mathcal{H}^{(i)}(t)/\partial \mathbf{u}]^{\mathsf{T}} [\partial \mathcal{H}^{(i)}(t)/\partial \mathbf{u}] \, \mathrm{d}t \right\}^{1/2} \leq \epsilon$$

and

$$\left\| \frac{\partial J^{(i)}}{\partial \mathbf{x}_o} \right\| = \left\{ \int_{t_o}^{t_f} [\partial J^{(i)}/\partial \mathbf{x}_o]^{\mathsf{T}} [\partial J^{(i)}/\partial \mathbf{x}_o] \, \mathrm{d}t \right\}^{1/2} \leq \epsilon,$$

where ϵ is a threshold value for the stopping criterion. Otherwise adjust the control sequence and parameter vector to

$$\mathbf{u}^{(i+1)}(t_k) = \mathbf{u}^{(i)}(t_k) - \kappa_u \frac{\partial \mathcal{H}^{(i)}}{\partial \mathbf{u}}(t_k), \quad k = 0, 1, \ldots, N-1$$

and

$$\mathbf{x}_o^{(i+1)} = \mathbf{x}_o^{(i)} - \kappa_{x_o} \frac{\partial J^{(i)}}{\partial \mathbf{x}_o},$$

where κ_u and κ_{x_o} are step sizes for the iterations in $\mathbf{u}$ and $\mathbf{x}_o$, respectively. Then set $\mathbf{x}_o^{(i)} \leftarrow \mathbf{x}_o^{(i+1)}$ and $\mathbf{u}^{(i)} \leftarrow \mathbf{u}^{(i+1)}$, and repeat steps 2–5.

In the present implementation, we evaluate $\partial \mathbf{f}/\partial \mathbf{x}$, $\partial \mathbf{f}/\partial \mathbf{u}$, and $\partial g/\partial \mathbf{x}$ by means of 8th-order central differences. Lower-order schemes were attempted as well, but the 8th-order scheme was the most consistent scheme in producing cost-minimizing results. The quantity $\partial g/\partial \mathbf{u}$ is analytically zero by definition of the impulse matching model. Although we could have discretized the control sequence by means of higher-order methods (e.g., higher-order interpolation or splines), we choose to employ the zero-order hold in the present implementation for the sake of simplicity. In the gradient descent step, we set $\kappa_u \sim \mathcal{O}(10^{-3})$ and $\kappa_{x_o} \sim \mathcal{O}(10^{-3})$ and adjust the values according to Armijo's rule (Nocedal and Wright, 2006). That is, we reduce the values of κ_u and κ_{x_o} by half until the cost at the next iteration $J^{(i+1)}$ yields a value smaller than the cost at the current iteration $J^{(i)}$. Finally, the empirical data $(F_x^{\text{true}}, F_y^{\text{true}})$ are interpolated to coincide with the time increments of the optimization routine. The vortex model and the type of maneuver under consideration dictate the maximum value of $\Delta t = t_{k+1} - t_k$, while numerical convergence and computational expense set a lower bound on Δt. By proceeding in this manner, the optimal solution can typically be attained in $\mathcal{O}(10^3)$–$\mathcal{O}(10^5)$ iterations of the algorithm, depending on the quality of the initial guess, the extent of the optimization time window, and the type of maneuver being considered.

3.3. True force histories: high-fidelity viscous vortex particle simulation

In the above formulation, we have assumed the existence of true force history data (i.e., F_x^{true} and F_y^{true}) with respect to which we minimize the error of our model predictions. For the purposes of the present study, we incorporate data from high-fidelity computations performed by way of the viscous vortex particle method (VVPM). The results of the VVPM computations have been verified against the experimental data of Granlund et al. (2010) for the case of a pitching plate (Wang and Eldredge, 2013). Details of the VVPM algorithm can be found in Eldredge (2007).

4. Results and discussion

The present section reports the results of the optimized impulse matching model for the cases of the pitch-up of a plate at steady traveling speed and an impulsively translating plate at a fixed angle of attack. We compare the results of the optimized model with high-fidelity VVPM simulation data and with the original impulse matching model (i.e., with the Kutta condition imposed at both the leading and trailing edges). We consider the pitch-up maneuver in Section 4.1 for pitching maneuvers of varying rates. The impulsively translating plate is studied in Section 4.2 for three different fixed angles of attack. In both cases, the optimization window begins after the plate has translated forward by 10% of a chord length.

4.1. Pitching kinematics

The pitching wing to be studied in this work is drawn schematically in Fig. 3. A two-dimensional wing profile of chord c, thickness $0.023c$, and semicircular edges translates rectilinearly at speed U_o in an incompressible flow with density ρ and kinematic viscosity ν. The wing undergoes a pitch-up maneuver at nominal angular velocity $\dot{\alpha}_o$ from 0° to 90° about an axis situated at the leading edge, with an angle of attack schedule, $\alpha(t)$, prescribed to be a smoothed linear ramp, as in Wang and Eldredge (2013). The nominal pitch rate, $\dot{\alpha}_o$, is specified via the dimensionless parameter $K = \dot{\alpha}_o c/(2U)$.

In the present study, we use high-fidelity VVPM data generated in Wang and Eldredge (2013). The Reynolds number, $\mathrm{Re} = Uc/\nu$, is fixed at 1000 for all high-fidelity simulations. The resulting drag and lift are scaled conventionally by $\rho U^2 c/2$ to form coefficients C_d and C_l, respectively.

4.1.1. Pitching kinematics: $K=0.2$

The drag and lift coefficients corresponding to the pitch-up maneuver of a flat plate are presented in Fig. 4 up to an angle of approximately 45°. The results of the optimized impulse matching model are presented alongside those of the high-fidelity simulation ($\mathrm{Re}=1000$) and the impulse matching model with Kutta condition imposed at both edges. We see that the optimized model performs significantly better than the original low-order model in reconstructing the force histories ($J^* = 1.3 \times 10^{-3}$ after 10^4 iterations). The accuracy of the optimized model's force reconstruction is quite remarkable, given

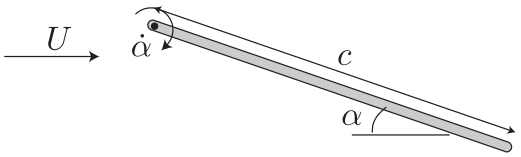

Fig. 3. Schematic of pitching wing.

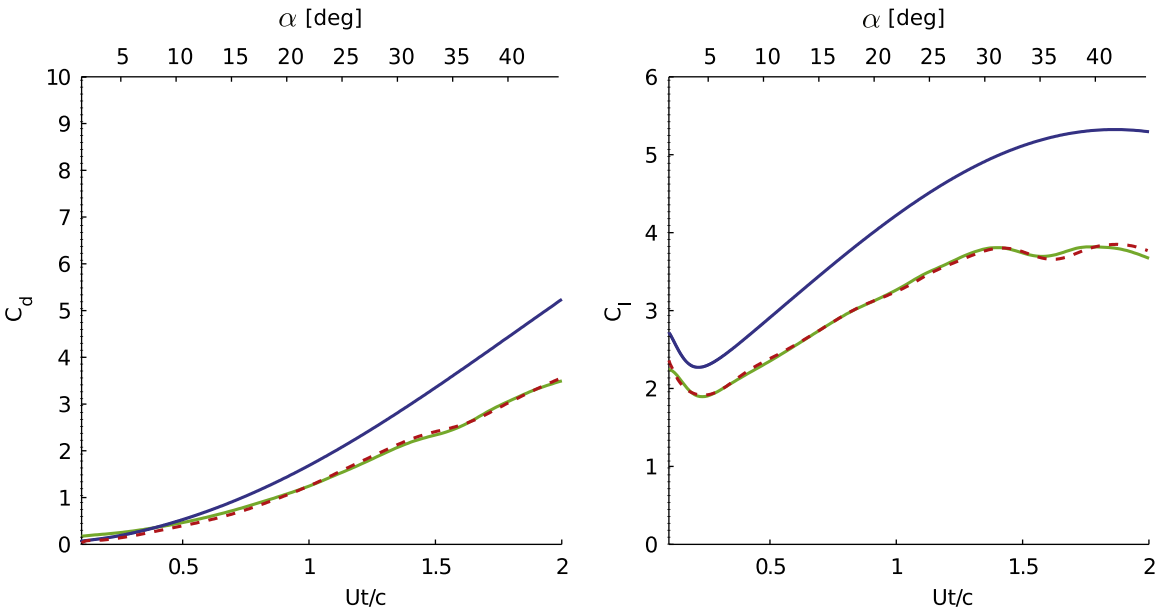

Fig. 4. Pitching plate ($K=0.2$) drag and lift coefficient histories associated with the VVPM data (—), the impulse matching model with Kutta conditions imposed at both the leading and trailing edge (—), and the optimized impulse matching model (- -).

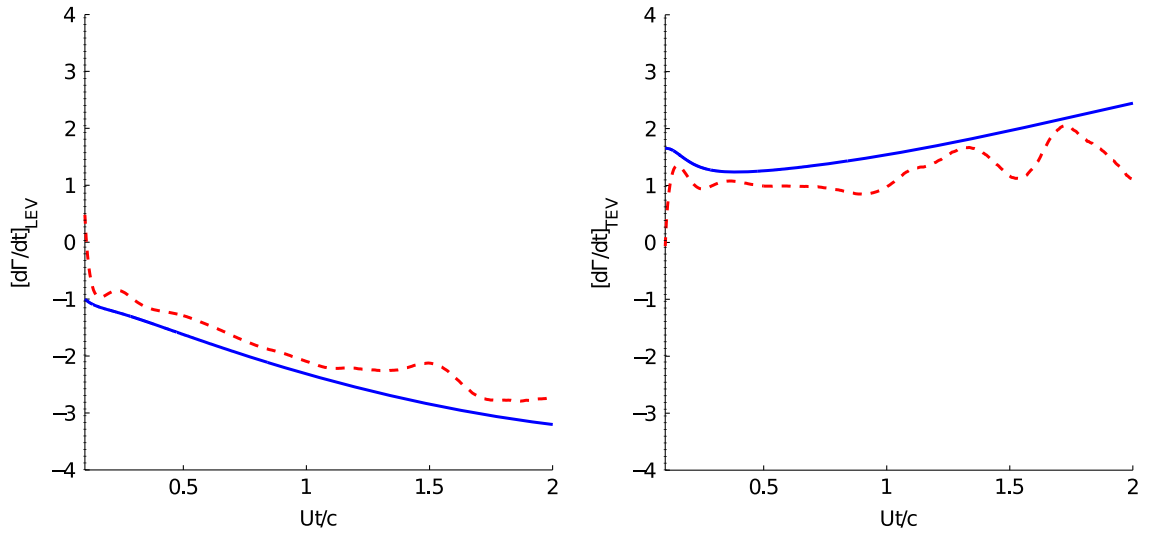

Fig. 5. Pitching plate ($K=0.2$) time rate of change of leading and trailing edge vortex strengths from the impulse matching model with Kutta conditions imposed at both the leading and trailing edge (–) and from the optimized impulse matching model (- -).

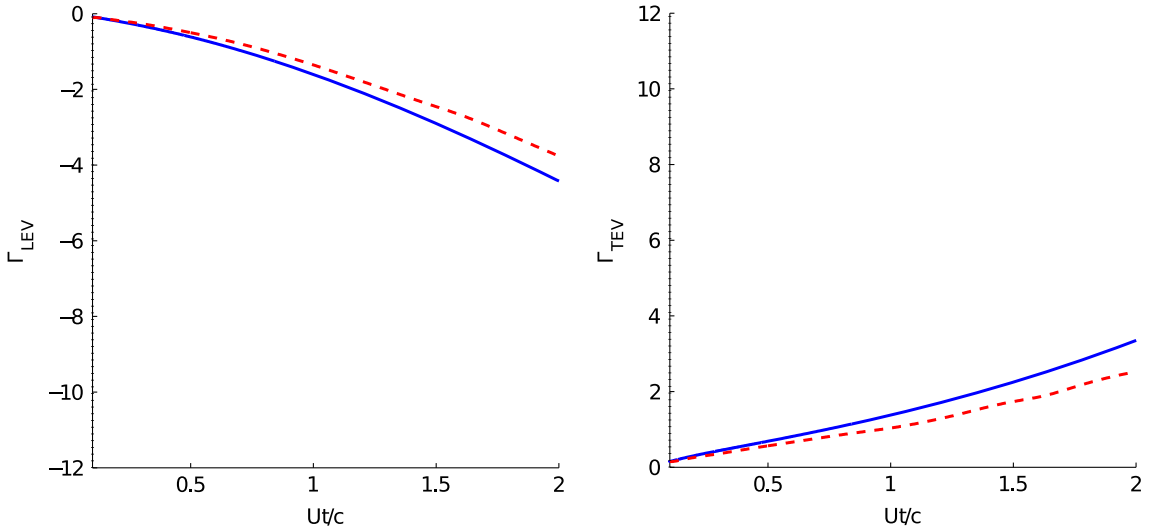

Fig. 6. Pitching plate ($K=0.2$) leading and trailing edge vortex strengths from the impulse matching model with Kutta conditions imposed at both the leading and trailing edge (–) and from the optimized impulse matching model (- -).

the fact that the low-order model possesses only six degrees of freedom, whereas the numerical simulation ultimately uses on the order of 5×10^5 computational particles, each with three degrees of freedom. It is worth noting that we performed the optimization procedure based on a variety of initial guesses, all of which yielded consistent solutions within numerical error. Although the optimization problem is non-convex, this observation indicates that the extremal solution is a strong local minimum. In the interest of reducing the convergence time, all of the results presented here are based on an initial guess corresponding to the original Kutta model.

Figs. 5–7 present the inputs and states of the system corresponding to the optimized model compared with the values resulting from the original model with Kutta conditions imposed. Fig. 5 presents the control input for both of these models, showing visible differences in the trends of $\dot{\Gamma}_{\mathrm{LEV}}$ and $\dot{\Gamma}_{\mathrm{TEV}}$. The time integrals of these inputs, the strengths themselves, exhibit significant differences with the original model predictions (c.f., Fig. 6). We see that the Kutta condition tends to over-predict the magnitude of the strength of both vortices. This is expected, since in reality there are viscous effects which mitigate the flux of vorticity in the vicinity of either edge, as seen in the VVPM results presented in Fig. 8. This is especially obvious at the leading edge where the LEV undergoes significant interaction with secondary vorticity of opposite sign. Fig. 7 presents the vortex trajectories in the physical plane. The difference in trajectories arises as a result of the difference in the evolution of the vortex strengths.

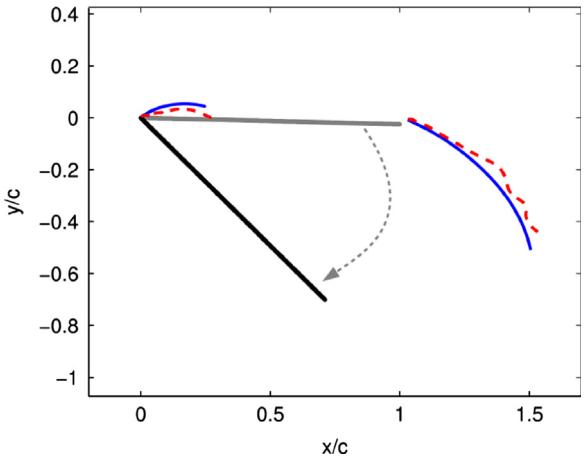

Fig. 7. Pitching plate ($K=0.2$) leading and trailing edge vortex trajectories from the impulse matching model with Kutta conditions imposed at both the leading and trailing edge (——) and from the optimized impulse matching model (- - -).

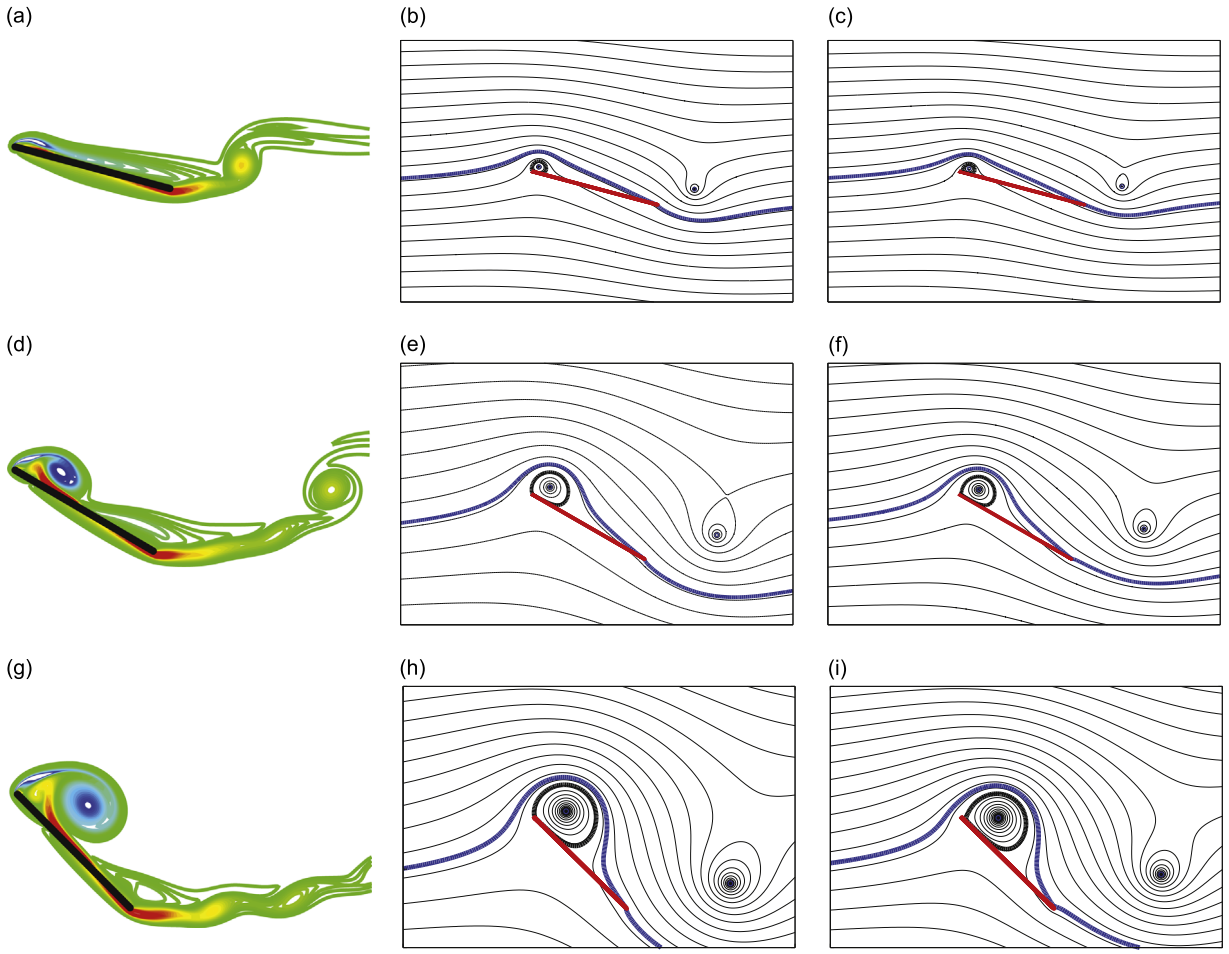

Fig. 8. Pitching plate ($K=0.2$) snapshots at $\alpha=15^\circ$, 30°, and 45°. The first column reports vorticity contours from the viscous vortex particle method (VVPM), while the second and third columns present streamlines from the original impulse matching model with a Kutta condition imposed (IMM) and the optimized impulse matching model (optimized IMM), respectively. Stagnation streamlines are drawn in bold. (a) VVPM ($\alpha=15^\circ$), (b) IMM ($\alpha=15^\circ$), (c) Optimized IMM ($\alpha=15^\circ$), (d) VVPM ($\alpha=30^\circ$), (e) IMM ($\alpha=30^\circ$), (f) Optimized IMM ($\alpha=30^\circ$), (g) VVPM ($\alpha=45^\circ$), (h) IMM ($\alpha=45^\circ$) and (i) Optimized IMM ($\alpha=45^\circ$),

Fig. 8 compares the streamlines of the optimized model with those of the original model at $\alpha = 15^\circ$, 30°, and 45° during the pitching motion. The vorticity contours from the high-fidelity VVPM simulations are also included for comparison. Inspection of the stagnation streamlines in the optimized model highlights the fact that the fore-wing stagnation point is slightly aft of the leading edge in the optimized model, not at the leading edge as constrained by a Kutta condition. The breakdown of the Kutta condition is expected for this maneuver since the flow structures in the vicinity of the leading edge do not resemble the release of a "smooth" thin sheet of vorticity from that edge, as seen in the vorticity contour plot from VVPM.

Based on the observation that the leading edge stagnation point is located slightly aft of the leading edge, it is natural to ask whether there is any advantage in imposing a modified Kutta condition. We examine this in a rudimentary manner by imposing the leading edge stagnation point location at various points along the fore-section of the wing while keeping the trailing edge stagnation point fixed at the trailing edge. We then compare the resulting forces from the impulse matching

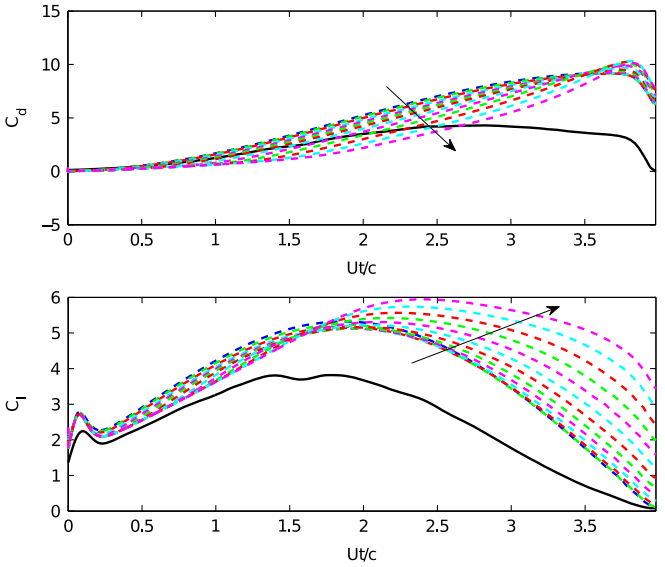

Fig. 9. Lift and drag histories associated with a pitch-up maneuver ($K=0.2$) using an impulse matching model with modified stagnation point specifications. The solid lines represent "true" forces, while the dashed lines correspond to model-predicted results using different regularity conditions. Only the leading edge stagnation point is varied here. The direction of the arrow corresponds to moving the leading edge stagnation point aftward, away from the leading edge.

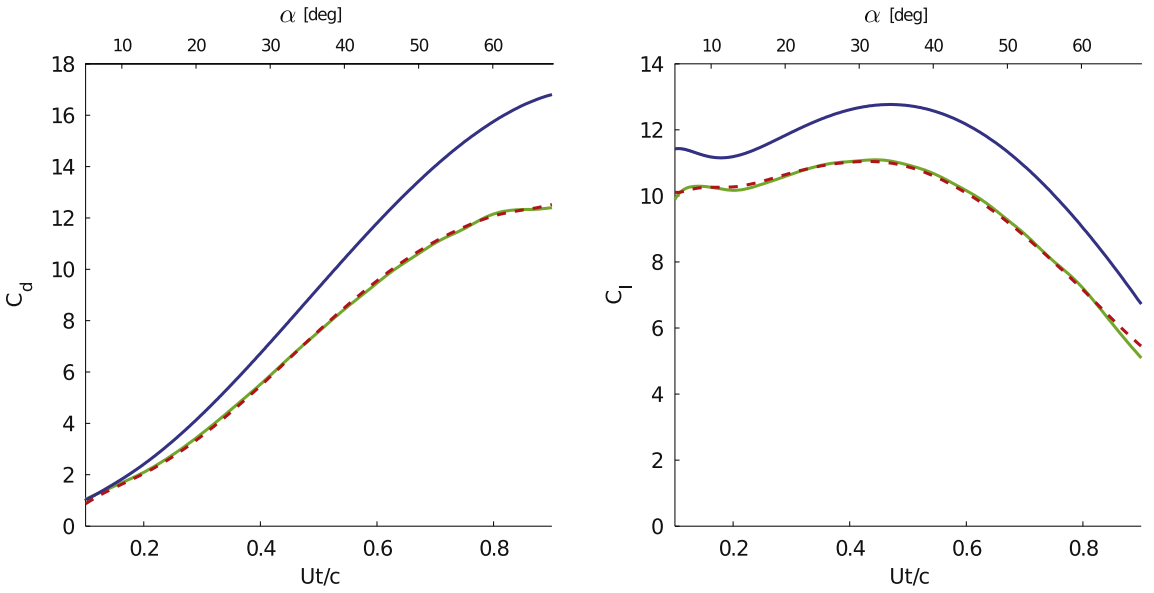

Fig. 10. Pitching plate ($K=0.7$) drag and lift coefficient histories associated with the VVPM data (–), the impulse matching model with Kutta conditions imposed at both the leading and trailing edge (–), and the optimized impulse matching model (- -).

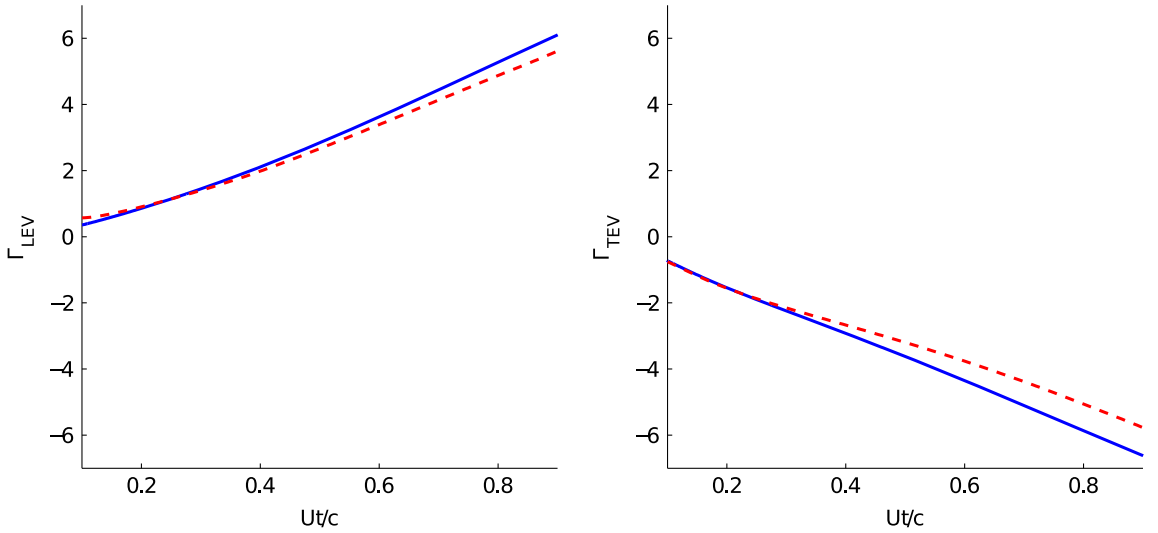

Fig. 11. Pitching plate ($K=0.7$) leading and trailing edge vortex strengths from the impulse matching model with Kutta conditions imposed at both the leading and trailing edge (—) and from the optimized impulse matching model (- -).

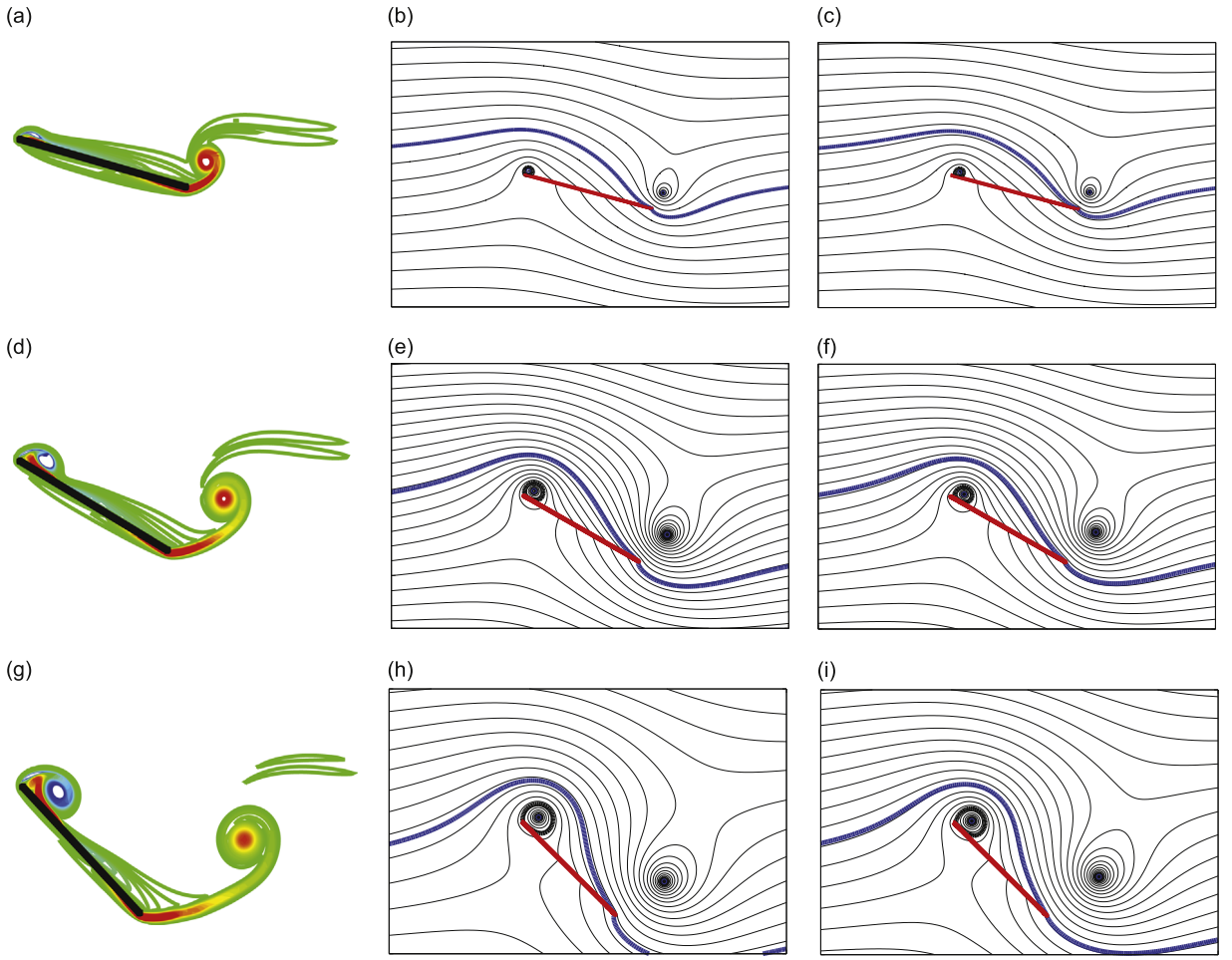

Fig. 12. Pitching plate ($K=0.7$) snapshots at $\alpha=15^\circ$, 30°, and 45°. The first column reports vorticity contours from the viscous vortex particle method (VVPM), while the second and third columns present streamlines from the original impulse matching model with a Kutta condition imposed (IMM) and the optimized impulse matching model (optimized IMM), respectively. Stagnation streamlines are drawn in bold. (a) VVPM ($\alpha=15^\circ$), (b) IMM ($\alpha=15^\circ$), (c) Optimized IMM ($\alpha=15^\circ$), (d) VVPM ($\alpha=30^\circ$), (e) IMM ($\alpha=30^\circ$), (f) Optimized IMM ($\alpha=30^\circ$), (g) VVPM ($\alpha=45^\circ$), (h) IMM ($\alpha=45^\circ$) and (i) Optimized IMM ($\alpha=45^\circ$),

model. As seen in Fig. 9, specifying a fixed stagnation point location alone is not sufficient for improving the original impulse matching model's force predictions. However, the results of the optimization procedure may inspire improved vortex strength models that deviate from the assumed form of (4), currently based on the Kutta condition.

4.1.2. Pitching kinematics: $K=0.7$

We now consider a more rapid pitch-up maneuver with $K=0.7$, for which the lift and drag coefficient time histories are presented in Fig. 10. Again, we see outstanding improvement compared to the original Kutta-based impulse matching model ($J^* = 3.3 \times 10^{-3}$ after 10^4 iterations).

Fig. 11 shows the strength histories corresponding to each model. As in the previous case, the Kutta condition over-predicts the magnitudes of these values. The discrepancy seems to be smaller for $K=0.7$ than for $K=0.2$ because the rapid pitch-up allows less time for viscous effects to play a dominant role, and more of the force is thus due to non-circulatory effects. This fact also accounts for the better accuracy of the force predictions from the original model for $K=0.7$ (Fig. 10) than for $K=0.2$ (Fig. 4). Comparisons of the model streamlines and VVPM vorticity contours are presented in Fig. 12. We report similar findings as with the $K=0.2$ pitch-up, namely that the fore-wing stagnation point is actually slightly aft of the leading edge in the optimized model. Additionally, this stagnation point tends to move about the fore-wing section throughout the maneuver, never locking in to a single position.

4.2. Impulsive translation

In the previous section, we considered the performance of the optimized model for the pitching problem, for which the aerodynamic forces consist of both inertial and circulatory contributions, and the leading-edge vortex develops in response to both translation and rotation relative to the surrounding fluid. In the present section, we explore the optimized model's performance in the simpler scenario of impulsive translation at a fixed angle of attack at $\mathrm{Re} = 1000$. This motion results in an infinitely large inertial reaction force at $t = 0^+$, but at all subsequent times the force is due almost entirely to circulatory effects (with the exception of drag at small angles, which is dominated by skin friction). For the purposes of the optimization, we consider minimizing the mean squared error between force histories after the plate has translated forward by 10% of a chord. We evaluate the optimized model for this problem at three different fixed angles of attack: 10°, 45°, and 90°.

4.2.1. Impulsive translation: $\alpha=10^\circ$

The resulting forces from the optimized model for 10° angle of attack are presented in Fig. 13. We find improvements in the lift reconstruction, but at the expense of the accuracy of the drag history. Since the impulse matching model does not account for skin friction drag, which is a dominant component at low angles of attack, this behavior does not come as a surprise. Such a viscous contribution would have to be accounted for separately, for example by incorporating the solution of the Rayleigh problem.

The streamlines for the optimized and original models, as well as the vorticity contours from VVPM, are presented in Fig. 14 for $Ut/c = 0.2$, 1.0, and 2.0. The stagnation streamline is overlaid in the vorticity contour plot for convenience.

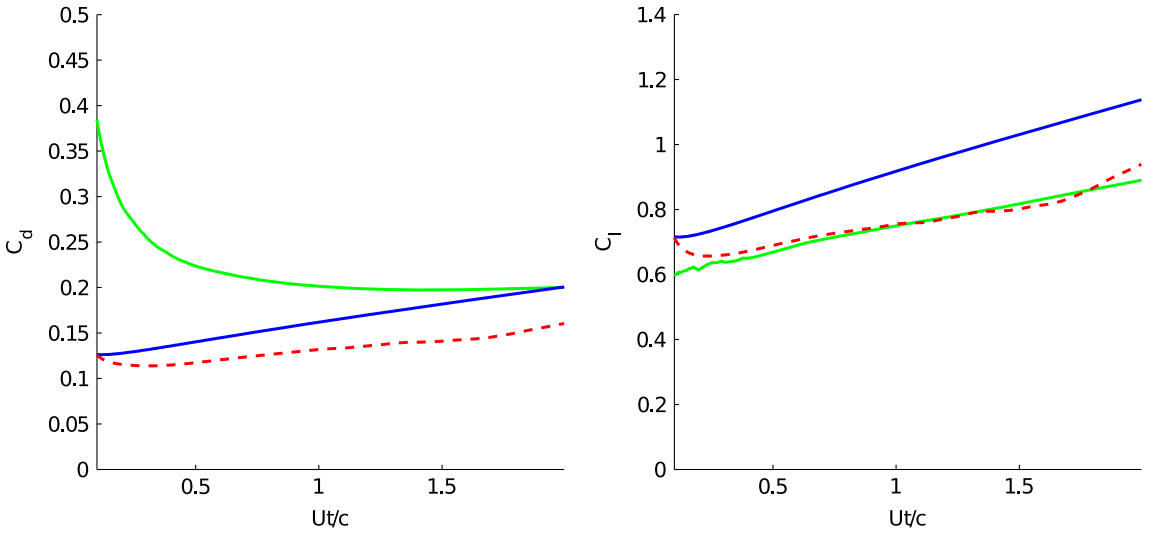

Fig. 13. Impulsively translating plate ($\alpha=10^\circ$) drag and lift coefficient histories associated with the VVPM data (—), the impulse matching model with Kutta conditions imposed at both the leading and trailing edge (—), and the optimized impulse matching model (- -).

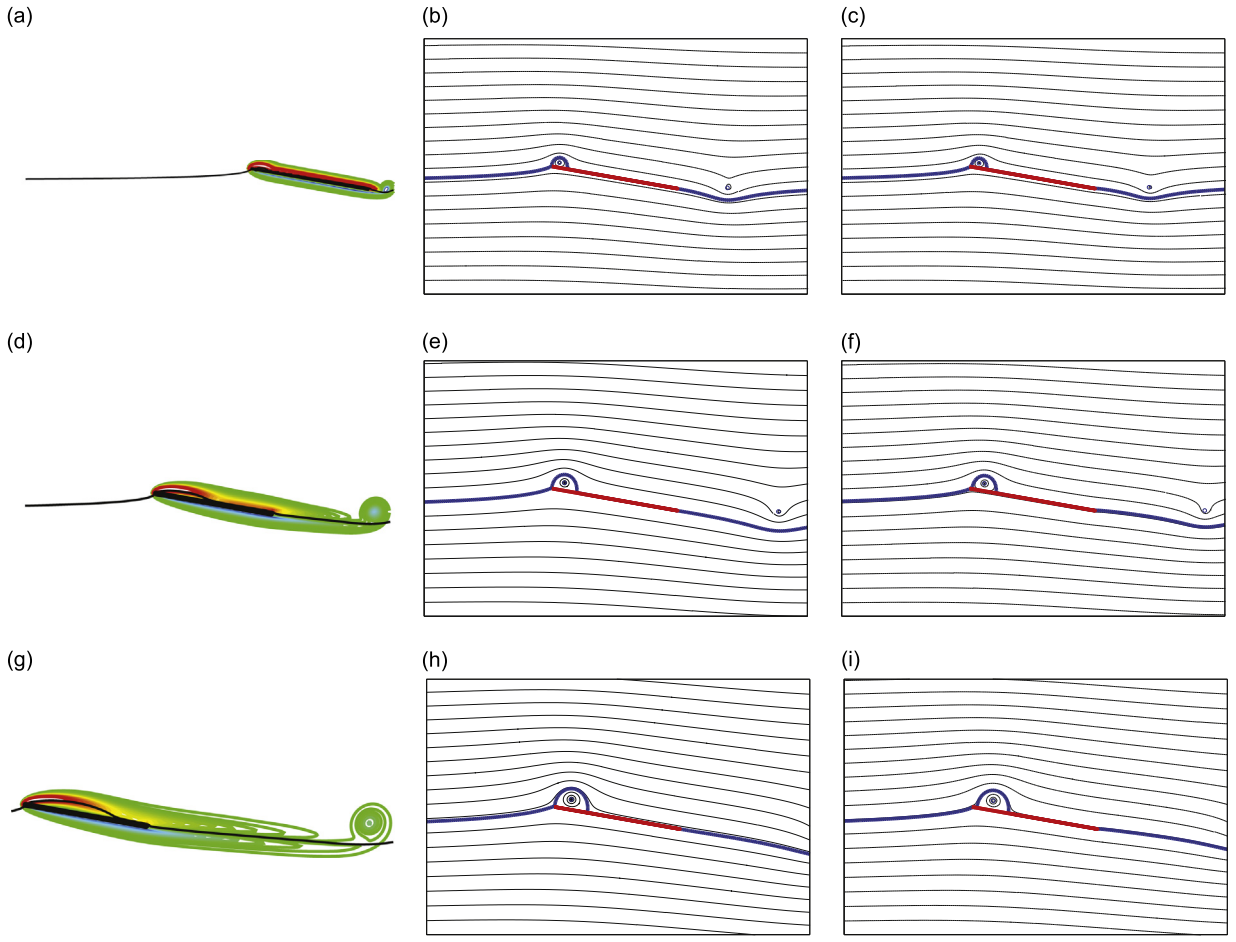

Fig. 14. Impulsively translating plate ($\alpha = 10^\circ$) at $Ut/c = 0.2$, 1.0, and 2.0. The first column reports vorticity contours from the viscous vortex particle method (VVPM), while the second and third columns present streamlines from the original impulse matching model with a Kutta condition imposed (IMM) and the optimized impulse matching model (optimized IMM), respectively. Stagnation streamlines are drawn in bold. (a) VVPM ($Ut/c = 0.2$), (b) IMM ($Ut/c = 0.2$), (c) Optimized IMM ($Ut/c = 0.2$), (d) VVPM ($Ut/c = 1.0$), (e) IMM ($Ut/c = 1.0$), (f) Optimized IMM ($Ut/c = 1.0$), (g) VVPM ($Ut/c = 2.0$), (h) IMM ($Ut/c = 2.0$) and (i) Optimized IMM ($Ut/c = 2.0$).

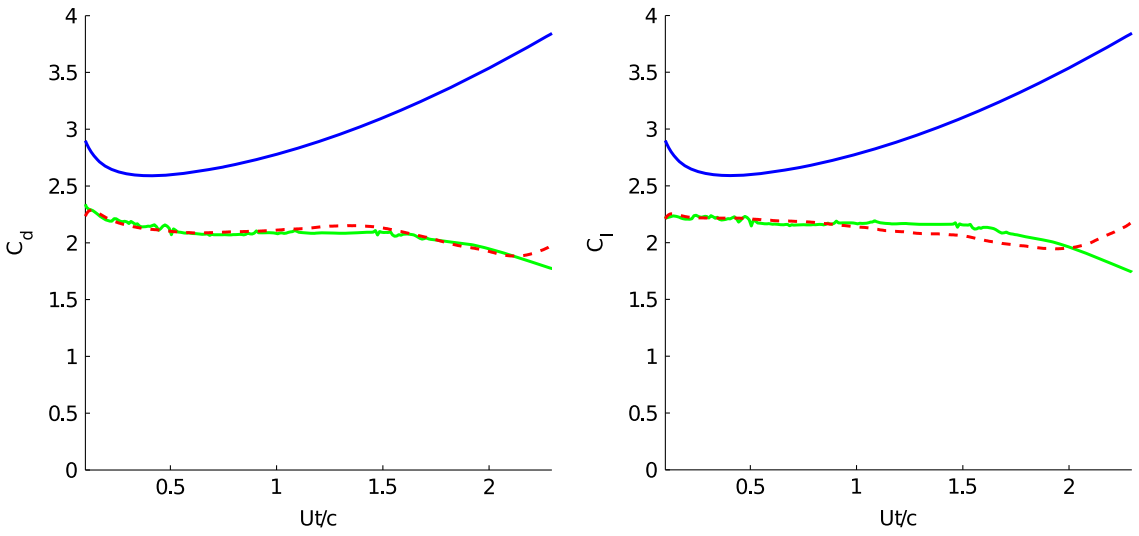

Fig. 15. Impulsively translating plate ($\alpha = 45^\circ$) drag and lift coefficient histories associated with the VVPM data (—), the impulse matching model with Kutta conditions imposed at both the leading and trailing edge (—), and the optimized impulse matching model (- -).

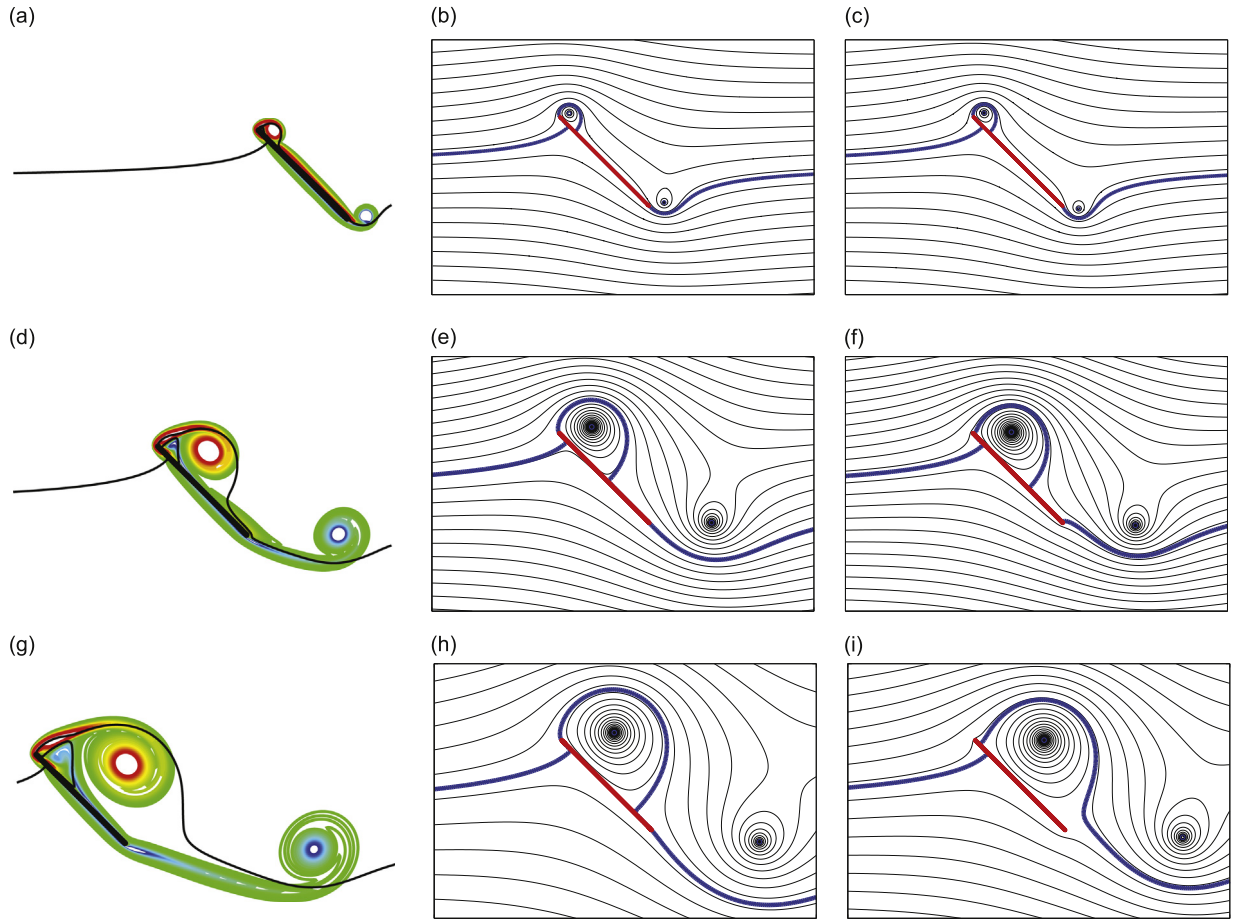

Fig. 16. Impulsively translating plate ($\alpha = 45^\circ$) at $Ut/c = 0.2$, 1.0, and 2.0. The first column reports vorticity contours from the viscous vortex particle method (VVPM), while the second and third columns present streamlines from the original impulse matching model with a Kutta condition imposed (IMM) and the optimized impulse matching model (optimized IMM), respectively. Stagnation streamlines are drawn in bold. (a) VVPM ($Ut/c = 0.2$), (b) IMM ($Ut/c = 0.2$), (c) Optimized IMM ($Ut/c = 0.2$), (d) VVPM ($Ut/c = 1.0$), (e) IMM ($Ut/c = 1.0$), (f) Optimized IMM ($Ut/c = 1.0$), (g) VVPM ($Ut/c = 2.0$), (h) IMM ($Ut/c = 2.0$) and (i) Optimized IMM ($Ut/c = 2.0$).

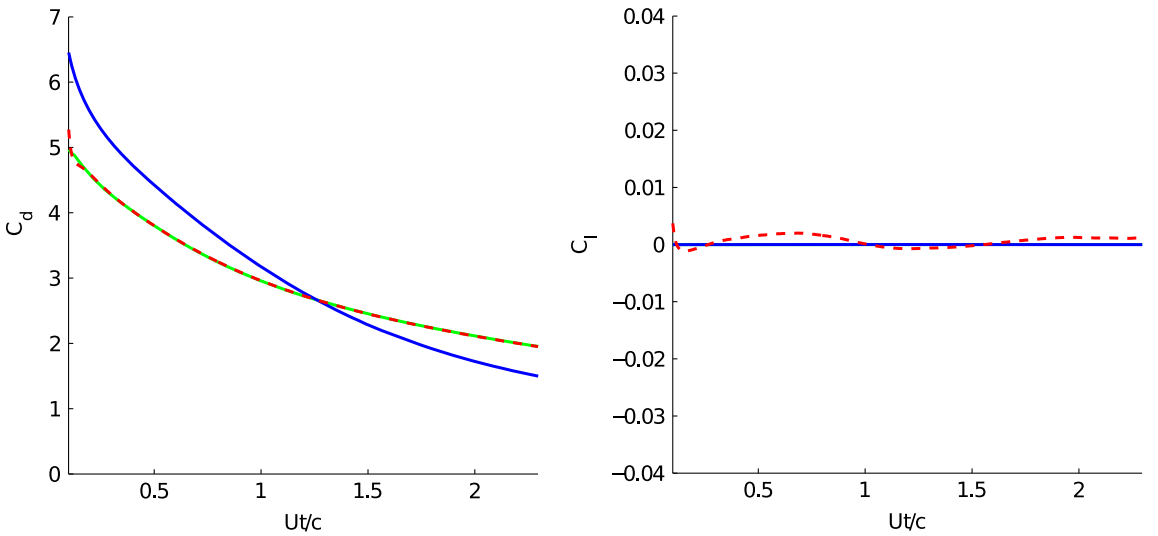

Fig. 17. Impulsively translating plate ($\alpha = 90^\circ$) drag and lift coefficient histories associated with the VVPM data (–), the impulse matching model with Kutta conditions imposed at both the leading and trailing edge (–), and the optimized impulse matching model (- -).

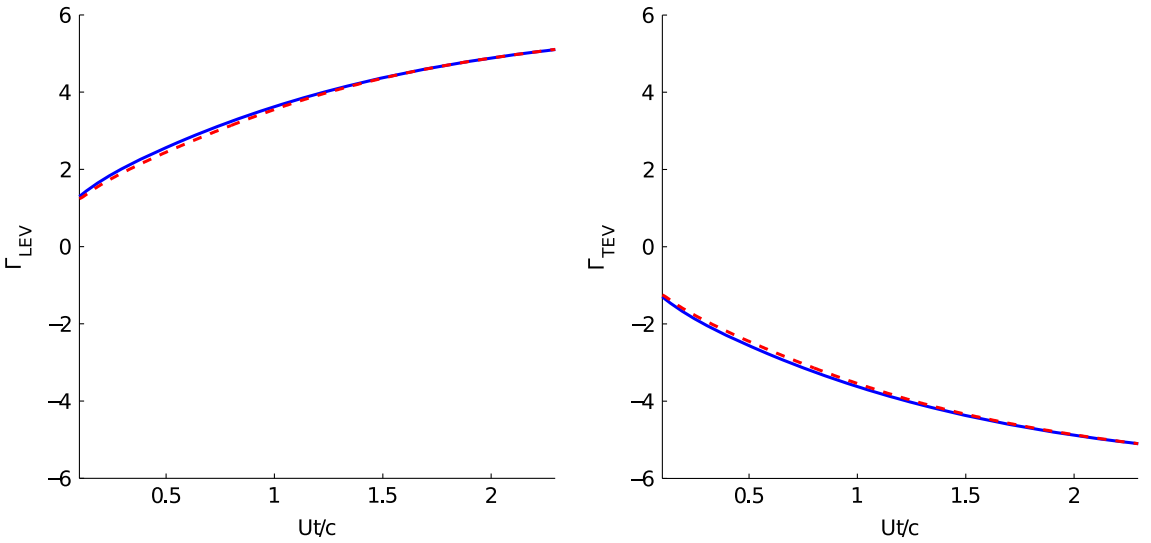

Fig. 18. Impulsively translating plate ($\alpha=90^\circ$) leading and trailing edge vortex strengths from the impulse matching model with the Kutta condition imposed at both the leading and trailing edge (–), and the optimized impulse matching model (- -).

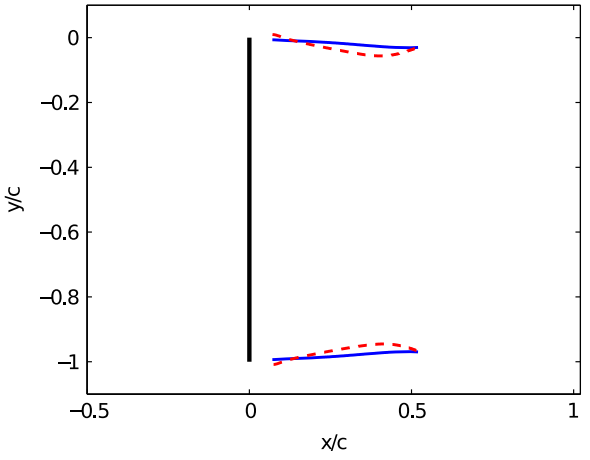

Fig. 19. Impulsively translating plate ($\alpha=90^\circ$) leading and trailing edge vortex trajectories from the impulse matching model with Kutta conditions imposed at both the leading and trailing edge (–) and from the optimized impulse matching model (- -).

4.2.2. *Impulsive translation: $\alpha=45^\circ$*

The optimized model performs remarkably better when circulatory effects outweigh skin friction effects, as seen in the force histories for the translating plate at $\alpha=45^\circ$ in Fig. 15. Despite the improvements attained through optimization ($J^* = 3.1 \times 10^{-3}$ in 10^5 iterations), the quality of the force reconstruction begins to deteriorate after about one chord-length of travel. The optimized model is able to capture this process, which is highlighted in bold in Fig. 16. However, the model does not replace the pinched-off TEV with a new vortex. It is evident from the VVPM vorticity contours and stagnation streamlines that the laminar separation bubble enclosing the LEV has burst at some point between $Ut/c = 1.0$ and 2.0. The initiation of this bursting process coincides with the deterioration in the model force reconstruction. Agreement for longer times would be enabled by initiating a new vortex from one or both edges.

4.2.3. *Impulsive translation: $\alpha=90^\circ$*

The case of a plate translating at 90° angle of attack results in excellent agreement between the optimized model and the high-fidelity force curves ($J^* = 7.1 \times 10^{-5}$ in 10^5 iterations), as shown in Fig. 17. The lift coefficient from the optimized model is slightly different from zero because we have not attempted to preserve symmetry during the optimization procedure. This can be confirmed by considering the resulting streamlines in Fig. 20. Though symmetry constraints could be imposed in the optimization problem formulation, doing so would take away from the generality of the approach.

The vortex strengths remain quite close to the Kutta predicted results, as seen in Fig. 18. A close examination of Fig. 20 does not reveal any notable difference between the stagnation point locations of the original and optimized models. The primary contributing factor in achieving better agreement in this configuration seems to be the initial positions of the edge vortices (c.f., Fig. 19).

5. Remaining challenges and paths to enhancement

Despite the progress made on vortex model optimization in the present study, several challenges remain to be addressed. In the present section, we address the issues of expanding the optimization time window and introducing subsequent vortex shedding within the optimization framework.

5.1. Convergence for large time windows and early times

All of the optimization results presented for the pitch-up maneuver in the previous section spanned a truncated time window. That is to say, the time window of optimization was not long enough to capture the full completion of the original pitch-up to 90°. Additionally, all of the optimizations of both pitch-up and impulsive translation were initiated when the wing had translated forward by 10% of its chord. From the experience gained in conducting the optimization procedure, it was determined that convergence was quite difficult for time windows larger than those reported. Moreover, if convergence did result with an extended time window, the resulting solution was often unsatisfactory and yielded a larger error than deemed acceptable.

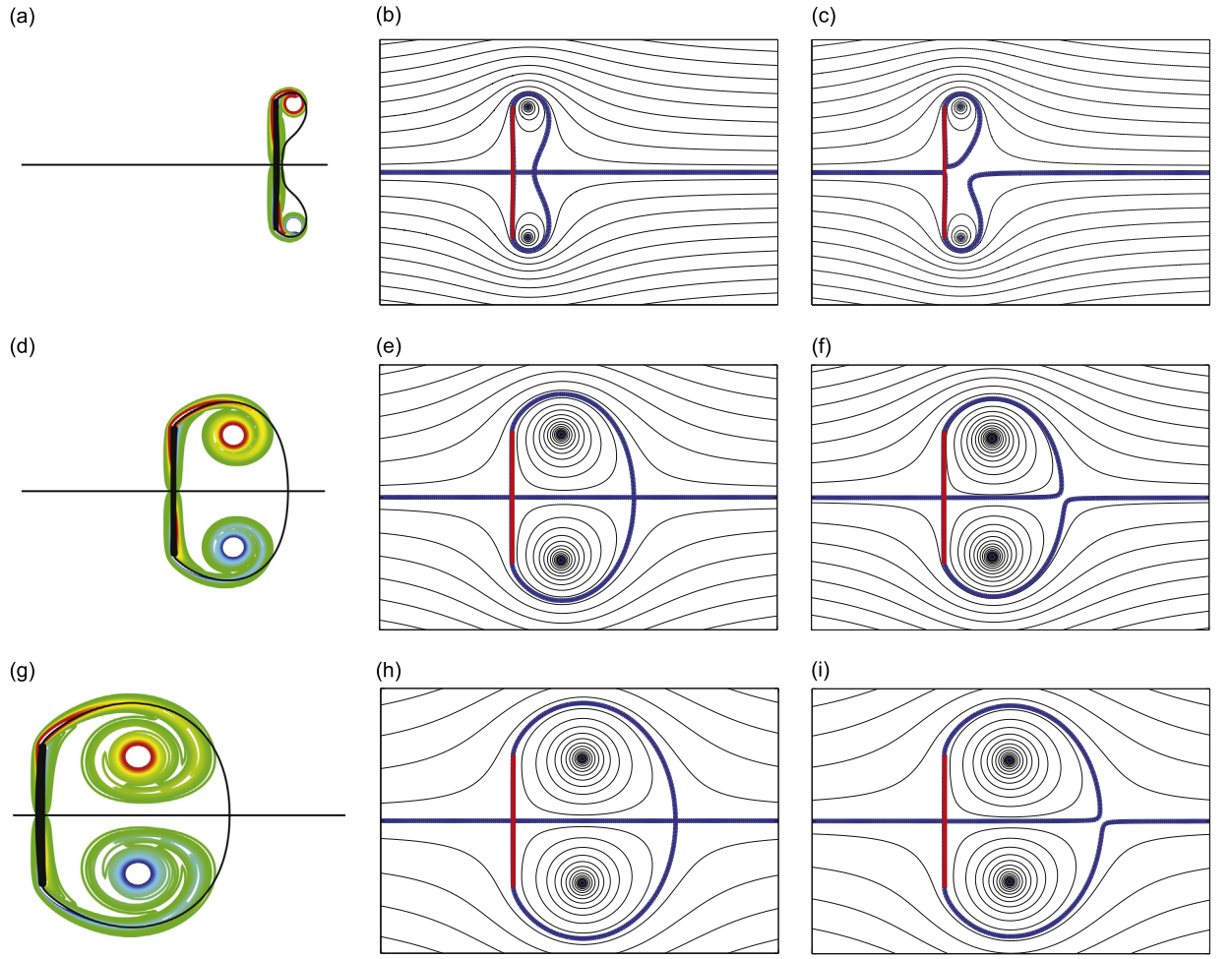

Fig. 20. Impulsively translating plate ($\alpha = 90^\circ$) at $Ut/c = 0.2$, 1.0, and 2.0. The first column reports vorticity contours from the viscous vortex particle method (VVPM), while the second and third columns present streamlines from the original impulse matching model with a Kutta condition imposed (IMM) and the optimized impulse matching model (optimized IMM), respectively. Stagnation streamlines are drawn in bold. (a) VVPM ($Ut/c = 0.2$), (b) IMM ($Ut/c = 0.2$), (c) Optimized IMM ($Ut/c = 0.2$), (d) VVPM ($Ut/c = 1.0$), (e) IMM ($Ut/c = 1.0$), (f) Optimized IMM ($Ut/c = 1.0$), (g) VVPM ($Ut/c = 2.0$), (h) IMM ($Ut/c = 2.0$) and (i) Optimized IMM ($Ut/c = 2.0$).

For the early-time behavior, part of the challenge can be attributed to the singular nature of the evolution equations at start-up. However, this does not fully account for the difficulty encountered, since acceptable results were difficult to attain for optimizations considering any time window beginning before 10% chord of travel. This is not to say that such results are impossible to attain; rather, the sensitivity of the results to the initial iteration of input history and parameter vector was too high to yield an improved model for this early-time window. This issue is more general: due to the highly nonlinear model, convergence is quite difficult for long time windows. In Section 5.2, we present a technique to address this concern, but first we provide a physical explanation for the origin of this difficulty.

One of the challenges with the later time behavior is the onset of vortex shedding. That is, there is an instant at which a developing point vortex should have its strength frozen, and a new vortex initiated from the corresponding edge. It is hypothesized that the vortex model would be able to better characterize the force response if a means of vortex shedding were included in the optimization model. A framework for introducing shedding into the vortex optimization framework will be discussed in Appendix A. However, this framework will highly depend upon the ability to treat early-time behavior. In the next section, we present a general strategy for extending the time window by means of stitching optimization.

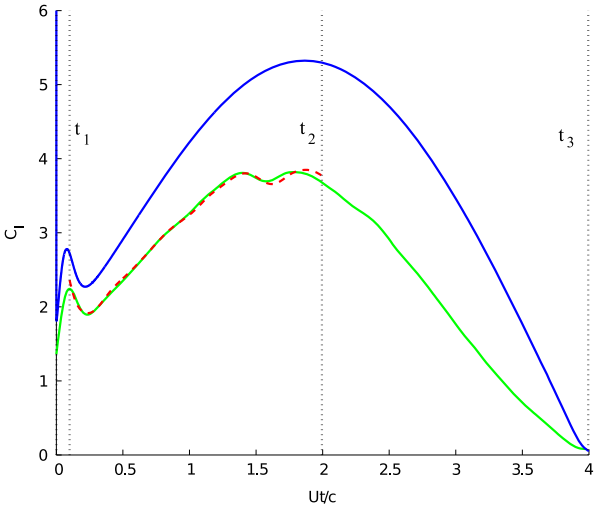

Fig. 21. The decomposition of the full time domain, $[t_o, t_f]$, into two smaller windows, $[t_1, t_2)$ and $[t_2, t_3]$. We currently assume that t_1 and t_2 are those corresponding to the time window for the original model optimization. Here we show the ($K = 0.2$) pitch-up maneuver lift history corresponding to the VVPM data (–), the impulse matching model with Kutta conditions imposed at both the leading and trailing edge (–), and the original optimized impulse matching model (- -).

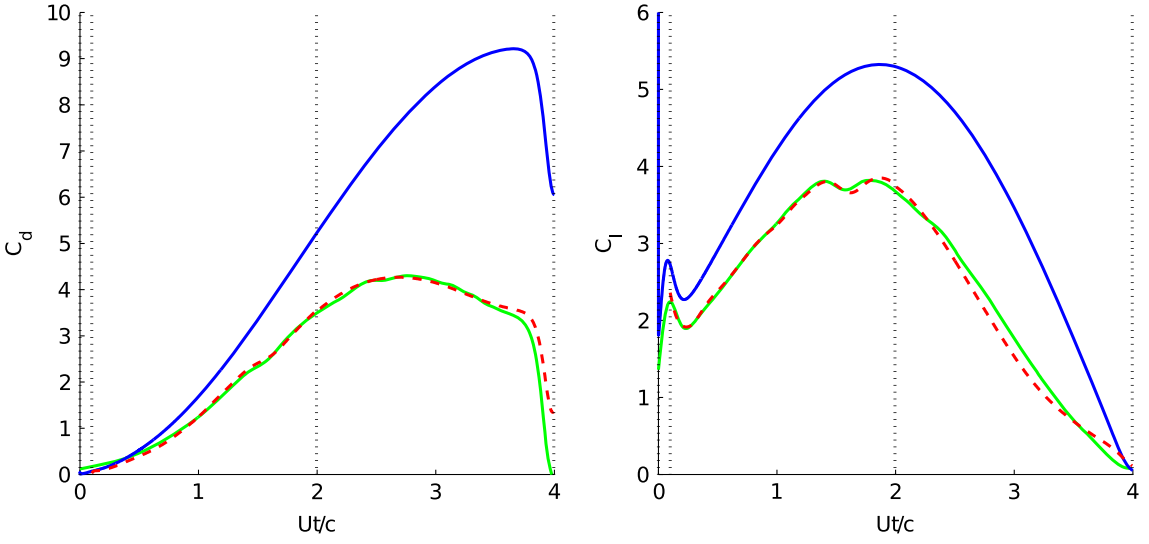

Fig. 22. Pitching plate (K=0.2) drag and lift coefficient histories associated with the VVPM data (–), the impulse matching model with Kutta conditions imposed at both the leading and trailing edge (–), and the stitch-optimized impulse matching model (- -).

5.2. Extending time windows via stitching

In the present section, we introduce a simple "stitching" method that can extend the time window of the optimization. The main premise of the proposed method is to divide the full time window into several more manageable ones. For the present study, we consider splitting the full time domain $[t_o, t_f]$ into two time windows $[t_1, t_2)$ and $[t_2, t_3]$, where $t_1, t_2, t_3 \in [t_o, t_f]$ (c.f., Fig. 21). Defining the intervals in this way is less restrictive than requiring $t_1 = t_o$ and $t_3 = t_f$ because it enables us to construct the time windows with favorable convergence characteristics. The vortex optimization procedure can then be applied to each of these time windows independently, coupled only by means of a continuity constraint on the trajectory of the state vector (i.e., $\mathbf{x}(t_2^+) = \mathbf{x}(t_2^-)$). Such an approach is slightly less restrictive than the original procedure in that it allows for discontinuities in the inputs at times corresponding to stitching instants (e.g., at $t = t_2$ in the present example). Additionally, the approach does not enforce continuity in the co-state $\mathbf{p}(t)$. In fact, the terminal value of the co-state, for a given time window, is always set to zero. As such the resulting stitched solution is not a true solution to the optimal control problem over the full time horizon. However, the stitching approach does lead to improved convergence properties and model predictions, thus making the procedure a useful tool for such analyses.

The results of the stitching procedure are reported in Figs. 22–27. For both $K=0.2$ and $K=0.7$, we have chosen t_1 and t_2 to correspond with the original vortex model optimization time windows considered in Section 4. We see that the later time

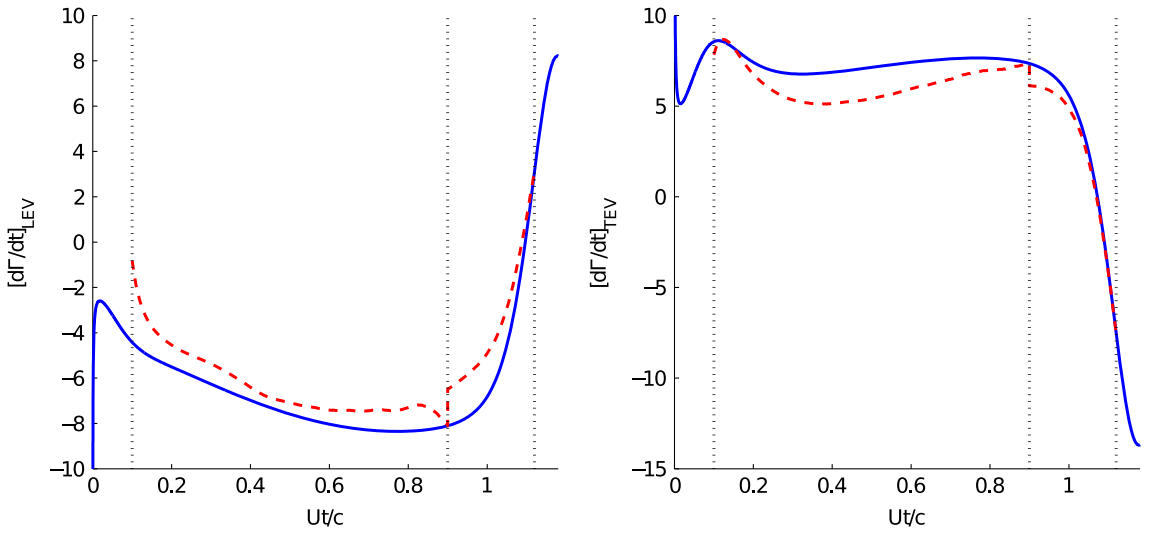

Fig. 23. Pitching plate ($K=0.2$) time rate of change of leading and trailing edge vortex strengths from the impulse matching model with Kutta conditions imposed at both the leading and trailing edge (—) and from the stitch-optimized impulse matching model (- -).

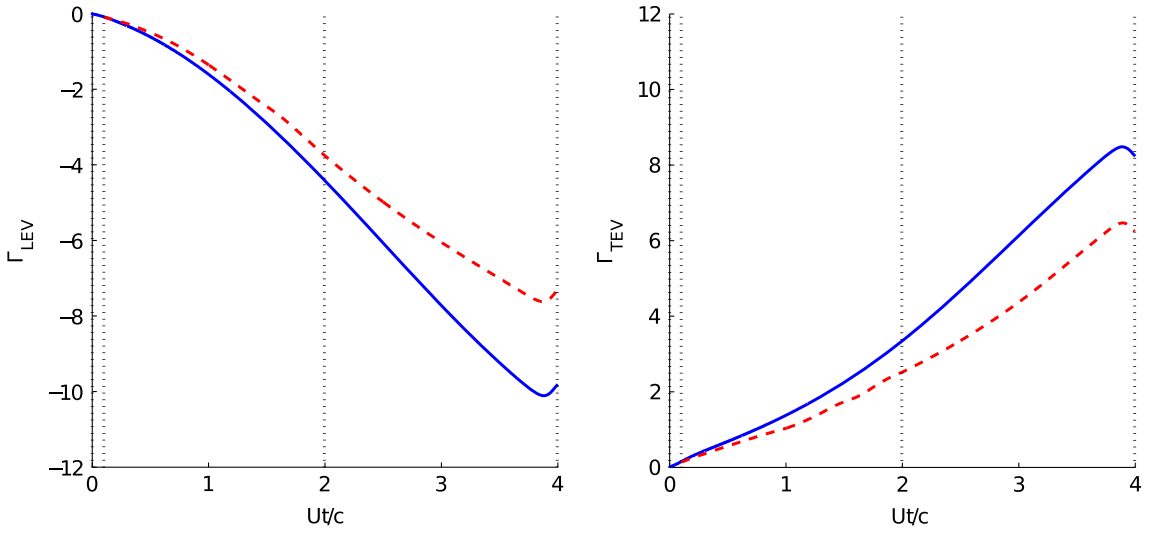

Fig. 24. Pitching plate ($K=0.2$) leading and trailing edge vortex strengths from the impulse matching model with Kutta conditions imposed at both the leading and trailing edge (—) and from the stitch-optimized impulse matching model (- -).

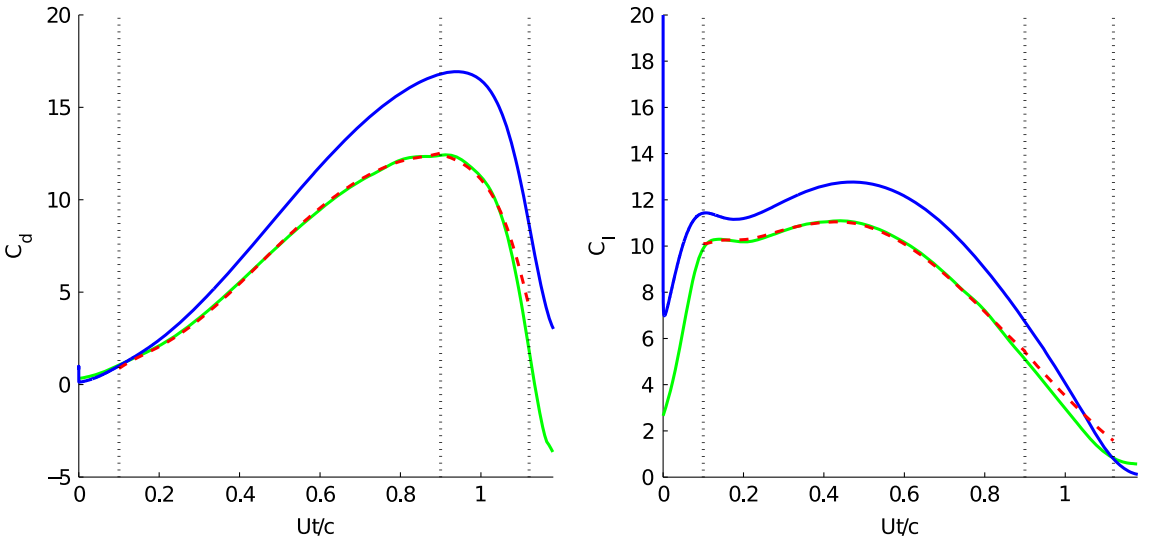

Fig. 25. Pitching plate ($K=0.7$) drag and lift coefficient histories associated with the VVPM data (—), the impulse matching model with Kutta conditions imposed at both the leading and trailing edge (—), and the stitch-optimized impulse matching model (- -).

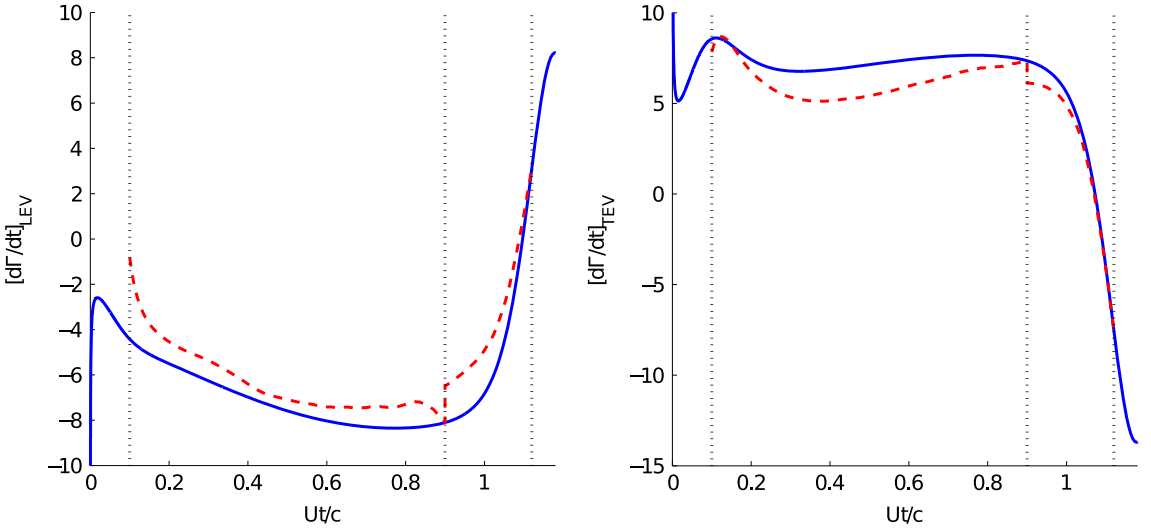

Fig. 26. Pitching plate ($K=0.7$) time rate of change of leading and trailing edge vortex strengths from the impulse matching model with Kutta conditions imposed at both the leading and trailing edge (—) and from the stitch-optimized impulse matching model (- -).

behavior is improved from the original impulse matching model, though the second time window tends to have a larger mean squared error than the first time window. This is expected since the triple (t_1, t_2, t_3) is chosen arbitrarily. The optimal input history is shown alongside the strength history to demonstrate that the discontinuity in the input at t_2 remains fairly small and does not affect the smoothness of the strength of either vortex. It must be noted that the impulse matching model is designed to allow such discontinuities in $\dot{\Gamma}_v$ without reflecting them in the force.

6. Conclusions

In this work, we have formulated a systematic framework for vortex model improvement based on variational principles and optimal control theory. We have demonstrated the optimization method's merits by demonstrating improvements to the impulse matching model, developed by Eldredge and Wang, for reconstructing the forces resulting from the pitching and/or translation of a two-dimensional plate. The force computations resulting from the optimized model match those predicted by high-fidelity simulations remarkably well for most of the flows considered. When they did not, it was because the underlying two-vortex model was insufficiently rich to capture the behavior (e.g., when the skin friction drag was a dominant factor and for flows undergoing subsequent vortex shedding). Despite these issues, the optimized model

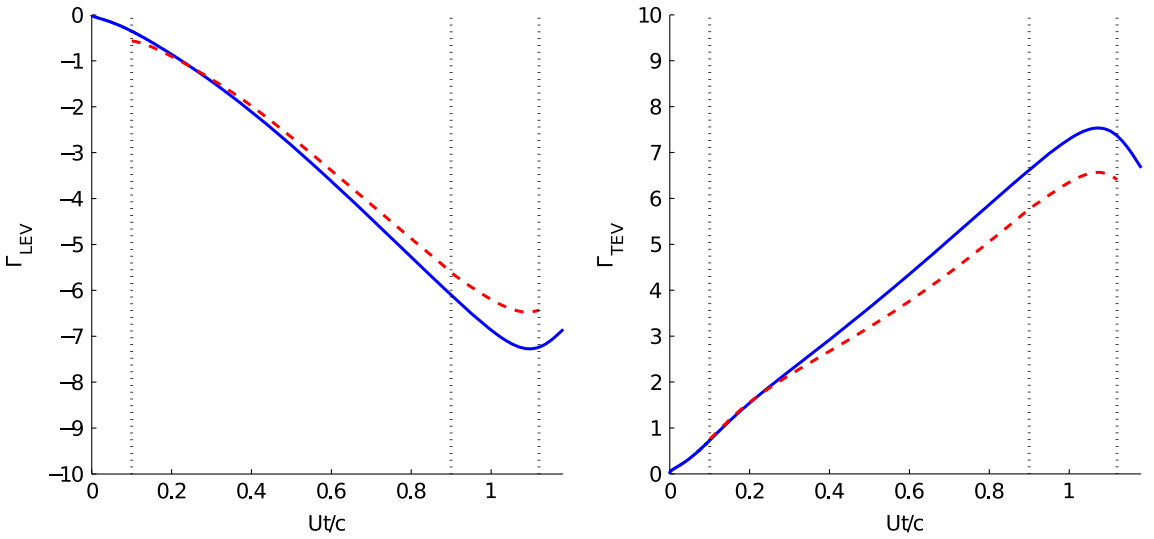

Fig. 27. Pitching plate ($K=0.7$) leading and trailing edge vortex strengths from the impulse matching model with Kutta conditions imposed at both the leading and trailing edge (—) and from the stitch-optimized impulse matching model (- -).

consistently predicted the forces better than the original impulse matching model for all the cases considered. Moreover, the quality of the results obtained using only six degrees of freedom is impressive, considering that the fully resolved high-fidelity simulations used between 10^5 and 10^6 degrees of freedom at $\mathrm{Re}=1000$.

Difficulties arose for convergence for early-time behavior as well as for extended time windows. In spite of the fact that the early-time issues have yet to be resolved, a "stitching" methodology was devised to allow the optimization to progress for extended time windows. The optimization framework developed here only represents a sample of the capabilities of the vortex model improvement paradigm. For example, the present method can be extended to incorporate subsequent vortex shedding during agile wing maneuvers, as discussed in Appendix A. Although we suggested techniques for accommodating vortex shedding within the optimization framework, practical implementation will require a better handling of early-time optimizations. Resolving vortex growth at early times remains the essential obstacle to be surmounted in the optimization, at least in the case of rapidly maneuvering wings.

The optimization framework demonstrates the capabilities of a two-vortex model in accurately reproducing the force histories of agile wing maneuvers. However, due to their non-autonomous nature, the resulting models are inadequate for force prediction and controller design on their own. Instead, the optimized vortex models offer insights into the shortcomings of the original vortex model and may guide improvements in future modeling efforts. Although we briefly considered developing an autonomous model based on our findings in Section 4.1.1, progress remains to be made on this front.

Ultimately, the model optimization framework developed here generalizes to other systems of interest, such as finite aspect ratio wings. To take such a step, however, will require the appropriate vortex models to represent such flows. Extensions to finite aspect ratio wings will likely expand upon unsteady modified lifting line (Jones, 1940; Dore, 1966) or vortex panel models, augmented with the development and influence of the LEV.

Acknowledgments

The authors gratefully acknowledge the support for this work from the Air Force Office of Scientific Research, Grant FA9550-11-1-0098 monitored by Dr. Douglas Smith.

A previous version of this work, Hemati et al. (2013), was presented at the 51st AIAA Aerospace Sciences Meeting (AIAA Paper 2013-0351).

Appendix A. A framework for subsequent vortex shedding

In Section 5.2, we demonstrated a method for overcoming some of the convergence challenges associated with large time windows. Despite this capability, it remains of interest to introduce a means of vortex shedding within the optimization framework. Not only will this provide potential for improving the predictions over the stitch-optimized results, but it also offers a means of gaining further physical insight into the nature of vortex shedding. We have already discussed the need to better handle early-time behavior before a successful vortex shedding optimization can be conducted. Nonetheless, we propose an approach for including vortex shedding such that it can be applied when the challenges associated with vortex start-up are resolved.

The problem of vortex shedding can be introduced into the current optimization framework by considering the shedding instant as an optimization parameter. This can be viewed in the same manner as the time domain decomposition into multiple time windows, as in the stitching case. However, now the second time window will follow the impulse matching evolution equations in the presence of an additional vortex, with a constant strength, while the first time window is treated as before. We will first consider the general framework of optimal model switching developed in Xu and Antsaklis (2004) in Appendix A.1, then in Appendix A.2 we discuss how this framework can be used to introduce vortex shedding within the optimization problem.

A.1. The optimal switching control problem

Consider the switched system consisting of the following subsystems:

$$\dot{\mathbf{x}} = \mathbf{f}_i(\mathbf{x}, \mathbf{u}), \quad \mathbf{f}_i: \mathbb{R}^n \times \mathbb{R}^m \to \mathbb{R}^n, \quad i \in I := \{1, 2, \ldots, M\}. \tag{A.1}$$

The optimal switching control problem consists of determining the optimal control input $\mathbf{u}^*$, in addition to an optimal switching sequence in $t \in [t_o, t_f]$ that specifies the sequence of active subsystems. This switching sequence is defined as

$$\sigma := ((t_o, i_o), (t_1, i_1), \ldots, (t_K, i_K)), \tag{A.2}$$

where $0 \le K < \infty$, $t_o \le t_1 \le \cdots \le t_K \le t_f$, and $i_k \in I$ for $k = 0, 1, \ldots, K$. Here, (t_k, i_k) denotes that at time t_k the system switched from subsystem i_{k-1} to subsystem i_k for the time interval $[t_k, t_{k+1})$ (except when $k=K$, for which the interval is $[t_K, t_f]$).

The optimal switching control problem can now be stated in the following manner. Consider a switched system consisting of subsystems $\dot{\mathbf{x}} = \mathbf{f}_i(\mathbf{x}, \mathbf{u})$, $i \in I$. Given a fixed time interval $[t_o, t_f]$ and a specified sequence of active subsystems $(i_o, i_1, \ldots, i_K)$, find a continuous input $u \in \mathcal{U}_{[t_o, t_f]}$ and switching instants $t_1, \ldots, t_K$ such that

$$J = \int_{t_o}^{t_f} g(\mathbf{x}, \mathbf{u})\, \mathrm{d}t \tag{A.3}$$

is minimized.

A.2. A framework to accommodate vortex shedding

In the spirit of the optimal switching control problem, we formulate a similar optimization problem for improving our vortex model by accounting for the shedding of multiple vortices. To do so, consider the switched system consisting of the following two subsystems, defined with respect to differing state and input vectors, $(\mathbf{x}_1, \mathbf{u}_1)$ and $(\mathbf{x}_2, \mathbf{u}_2)$

$$\dot{\mathbf{x}}_1 = \mathbf{f}_1(\mathbf{x}_1, \mathbf{u}_1), \quad t \in [t_o, t_1), \tag{A.4}$$

$$\dot{\mathbf{x}}_2 = \mathbf{f}_2(\mathbf{x}_2, \mathbf{u}_2), \quad t \in [t_1, t_f]. \tag{A.5}$$

The switching sequence here is simply $\sigma = ((t_o, i_o), (t_1, i_1))$ since the subsystems will only switch once. We have intentionally made a distinction between (x_1, u_1) and (x_2, u_2) in an effort to emphasize, from a modeling standpoint, the release of one vortex "in exchange for" the introduction of another. The problem now is to determine the inputs u_1 and u_2, the initial conditions on the states $\mathbf{x}_1^o = \mathbf{x}_1(t_o)$ and $\mathbf{x}_2^o = \mathbf{x}_2(t_1)$, and the switching instant t_1, such that

$$J = \int_{t_o}^{t_1} g(\mathbf{x}_1, \mathbf{u}_1)\, \mathrm{d}t + \int_{t_1}^{t_f} g(\mathbf{x}_2, \mathbf{u}_2)\, \mathrm{d}t \tag{A.6}$$

is minimized.

We can rewrite this last statement as

$$\min_{\mathbf{u}_1, \mathbf{u}_2, \mathbf{x}_1^o, \mathbf{x}_2^o, t_1} J = \min_{\mathbf{u}_1, \mathbf{u}_2, \mathbf{x}_1^o, \mathbf{x}_2^o, t_1} \left[\int_{t_o}^{t_1} g(\mathbf{x}_1, \mathbf{u}_1)\, \mathrm{d}t + \int_{t_1}^{t_f} g(\mathbf{x}_2, \mathbf{u}_2)\, \mathrm{d}t \right], \tag{A.7}$$

$$\min_{\mathbf{u}_1, \mathbf{u}_2, \mathbf{x}_1^o, \mathbf{x}_2^o, t_1} J = \min_{t_1} \left\{ \min_{\mathbf{u}_1, \mathbf{u}_2, \mathbf{x}_1^o, \mathbf{x}_2^o} \left[\int_{t_o}^{t_1} g(\mathbf{x}_1, \mathbf{u}_1)\, \mathrm{d}t + \int_{t_1}^{t_f} g(\mathbf{x}_2, \mathbf{u}_2)\, \mathrm{d}t \right] \right\}, \tag{A.8}$$

$$\min_{\mathbf{u}_1, \mathbf{u}_2, \mathbf{x}_1^o, \mathbf{x}_2^o, t_1} J = \min_{t_1} \left\{ \min_{\mathbf{u}_1, \mathbf{x}_1^o} \int_{t_o}^{t_1} g(\mathbf{x}_1, \mathbf{u}_1)\, \mathrm{d}t + \min_{\mathbf{u}_2, \mathbf{x}_2^o} \int_{t_1}^{t_f} g(\mathbf{x}_2, \mathbf{u}_2)\, \mathrm{d}t \right\}. \tag{A.9}$$

Though the original form should be used for practical implementation, writing the minimization in this form demonstrates the equivalent nature of the problem to the optimization we have already considered. That is, this "switching" problem nests two optimization problems with the same form we treated previously, with an additional parameter optimization for t_1.

It should be noted that this framework can be extended arbitrarily to accommodate any number of vortex shedding events. Of course the practicality of computing a solution for multiple shedding events may be a limiting factor. In addition to convergence properties having a greater potential for being poor, the computational expense grows with the addition of each switching event. Even if we ignore the detrimental effects of a larger time horizon to bring about more switching

events, this statement remains true because each additional switching event requires an additional parameter optimization on the switching instant t_k.

References

Alben, S., Shelley, M.J., 2008. Flapping states of a flag in an inviscid fluid: bistability and the transition to chaos. Physical Review Letters 100, 074301.

Ansari, S.A., Zbikowski, R., Knowles, K., 2006. Non-linear unsteady aerodynamic model for insect-like flapping wings in the hover. Part 1. Methodology and analysis. Proceedings IMechE, Part G: Journal of Aerospace Engineering 220 (G2), 61–83.

Brown, C.E., Michael, W.H., 1954. Effect of leading edge separation on the lift of a delta wing. Journal of the Aeronautical Sciences 21, 690–694.

Brunton, S.L., Rowley, C.W., 2011. Low-dimensional representations for classical unsteady aerodynamic models. In: AIAA Paper 2011-476. 49th AIAA Aerospace Sciences Meeting, Orlando, FL.

Brunton, S.L., Rowley, C.W., 2013. Empirical state-space representations of Theodorsen's lift model. Journal of Fluids and Structures 38, 174–186.

Bryson, A.E., Ho, Y.-.C., 1975. Applied Optimal Control. Hemisphere Publishing Corp., Washington, DC.

Cortelezzi, L., Leonard, A., 1993. Point vortex model of the unsteady separated flow past a semi-infinite plate with transverse motion. Fluid Dynamics Research 11, 263–295.

Dore, B.D., 1966. The Unsteady Forces on Finite Wings in Transient Motion. Technical Report 3456. Ministry of Aviation Aeronautical Research Council.

Eldredge, J.D., 2007. Numerical simulation of the fluid dynamics of 2D rigid body motion with the vortex particle method. Journal of Computational Physics 221, 626–648.

Eldredge, J.D., Wang, C., 2010. High fidelity simulations and low-order modeling of a rapidly pitching plate. In: AIAA Paper 2010-4281. 40th AIAA Fluid Dynamics Conference and Exhibit. Chicago, IL.

Garrick, I.E., 1937. Propulsion of a Flapping and Oscillating Airfoil. Technical Report 567. NACA.

Graham, J.M.R., 1980. The forces on sharp-edged cylinders in oscillatory flow at low Keulegan–Carpenter numbers. Journal of Fluid Mechanics 97 (1), 331–346.

Granlund, K., Ol, M.V., Garmann, D.J., Visbal, M.R., Bernal, L., 2010. Experiments and computations on abstractions of perching. In: AIAA Paper 2010-4943. 48th AIAA Applied Aerodynamics Conference, Chicago, IL.

Hemati, M.S., Eldredge, J.D., Speyer, J.L., 2013. Improving vortex models via optimal control theory. In: AIAA Paper 2013-0351. 51st AIAA Aerospace Sciences Meeting, Grapevine, TX.

Jones, K.D., Platzer, M.F., 2000. Flapping-wing propulsion for micro air vehicle. in: AIAA Paper 2000-0897. 38th AIAA Aerospace Sciences Meeting, Reno, NV.

Jones, M.A., 2003. The separated flow of an inviscid fluid around a moving flat plate. Journal of Fluid Mechanics 496, 405–441.

Jones, R.T., 1940. The Unsteady Lift of a Wing of Finite Aspect Ratio. Technical Report 681. NACA.

Katz, J., Weihs, D., 1978. Behavior of vortex wakes from oscillating airfoils. AIAA Journal 15 (12), 861–863.

Kirk, D.E., 2004. Optimal Control Theory: An Introduction. Dover Publications, Mineola, NY.

Krasny, R., 1991. Vortex sheet computations: roll-up, wakes, separation. In: Anderson, C.R., Greengard, C. (Eds.), Lectures in Applied Mathematics, vol. 28. Applied Mathematical Society, Seattle, WA, pp. 385–402.

Leishman, J.G., Beddoes, T.S., 1989. A semi-empirical model for dynamic stall. Journal of the American Helicopter Society 34 (3), 3–17.

Michelin, S., Llewelyn Smith, S.G., 2009. An unsteady point vortex method for coupled fluid–solid problems. Theoretical and Computational Fluid Dynamics 23, 127–153.

Nitsche, M., Krasny, R., 1994. A numerical study of vortex ring formation at the edge of a circular tube. Journal of Fluid Mechanics 276, 139–161.

Nocedal, J., Wright, S.J., 2006. Numerical Optimization, second ed. Springer, New York.

Pitt Ford, C.W., Babinsky, H., 2013. Lift and the leading-edge vortex. Journal of Fluid Mechanics 720, 280–313.

Pullin, D.I., Wang, Z.J., 2004. Unsteady forces on an accelerating plate and application to hovering insect flight. Journal of Fluid Mechanics 509, 1–21.

Ramesh, K., Gopalarathnam, A., Edwards, J.R., 2012. Theoretical modeling of leading edge vortices using the leading edge suction parameter. In: AIAA Paper 2012-3027. 30th AIAA Applied Aerodynamics Conference, New Orleans, LA.

Ramesh, K., Gopalarathnam, A., Edwards, J.R., Ol, M.V., Granlund, K., 2013. An unsteady airfoil theory applied to pitching motions validated against experiment and computation. Theoretical and Computational Fluid Dynamics 27 (6), 843–864.

Shukla, R.K., Eldredge, J.D., 2007. An inviscid model for vortex shedding from a deforming body. Theoretical and Computational Fluid Dynamics 21, 343–368.

Speyer, J.L., Jacobson, D.H., 2010. Primer on Optimal Control Theory. SIAM, Philadelphia.

Taha, H.E., Hajj, M.R., Beran, P.S., 2013. Unsteady nonlinear aerodynamics of hovering MAVs/insects. In: AIAA Paper 2013-0504. 51st AIAA Aerospace Sciences Meeting, Grapevine, TX.

Theodorsen, T., 1935. General Theory of Aerodynamic Instability and the Mechanism of Flutter. Technical Report 496. NACA.

von Kármán, T., Sears, W.R., 1938. Airfoil theory for non-uniform motion. Journal of the Aeronautical Sciences 5 (10), 379–390.

Wagner, H.A., 1925. Über die Enstehung des dynamischen Auftriebes von Tragflügeln. Zeitschrift für Angewandte Mathematik und Machanik 5 (1), 17–35.

Wang, C., Eldredge, J.D., 2013. Low-order phenomenological modeling of leading-edge vortex formation. Theoretical and Computational Fluid Dynamics 27 (5), 577–598.

Wong, J.G., Kriegseis, J., Rival, D.E., 2013. An investigation into vortex growth and stabilization for two-dimensional plunging and flapping with varying sweep. Journal of Fluids and Structures 43, 231–243.

Xia, X., Mohseni, K., 2013. Lift evaluation of a two-dimensional pitching flat plate. Physics of Fluids 25 (9), 091901.

Xu, X., Antsaklis, P.J., 2004. Optimal control of switched systems based on parameterization of the switching instants. IEEE Transactions on Automatic Control 49 (1), 2–16.